Fast Laser Scan Matching using Polar Coordinates

Albert Diosi and Lindsay Kleeman
ARC Centre for Perceptive and Intelligent Machines in Complex Environments
Department of Electrical and Computer Systems Engineering
Monash University, Clayton, VIC 3168, Australia
albert.diosi@gmail.com
Lindsay.Kleeman@eng.monash.edu.au

June 12, 2007

Abstract

In this paper a novel Polar Scan Matching (PSM) approach is described that works in the laser scanner's polar coordinate system, therefore taking advantage of the structure of the laser measurements and eliminates the need for an expensive search for corresponding points in other scan match approaches. PSM belongs to the family of point to point scan matching approaches with its matching bearing association rule. The performance of PSM is thoroughly evaluated in a simulated experiment, in experiments using ground truth, in experiments aimed at determining the area of convergence and in a SLAM experiment. All results are compared to results obtained using an iterated closest point (ICP) scan matching algorithm implementation. It is found that PSM is superior to the ICP implementation in processing speed and that PSM converges to a correct solution from a larger range of initial positions.

1 Introduction

Localization and map making is an important function of mobile robots. One possible way to assist with this functionality is to use laser scan matching. A 2D laser scan is a set of range measurements with constant angle increment taken in a horizontal plane. In laser scan matching, the position and orientation or pose of the current scan is sought with respect to a reference laser scan by adjusting the pose of the current scan until the best overlap with the reference scan is achieved. In the literature there are methods for 2D and 3D scan matching. This paper restricts discussion to 2D laser scan matching.

Scan matching approaches can be local [Lu and Milios, 1997] or global [Tomono, 2004]. When performing local scan matching, two scans are matched while starting from an initial pose estimate. When performing global scan matching the current scan is aligned with respect to a map or a database of scans without the need to supply an initial pose estimate. Scan matching approaches also can be categorized based on their association method such as feature to feature, point to feature and point to point. In feature to feature matching approaches, features such as line segments [Gutmann, 2000], corners or range extrema [Lingemann *et al.*, 2004] are extracted from laser scans, and then matched. Such approaches interpret laser scans and require the presence of chosen features in the environment. In point to feature approaches, such as one of the earliest by Cox [1991], the points of a scan are matched to features such as lines. The line features can be part of a predefined map. Features can be more abstract as in [Biber and Straßer, 2003], where features are Gaussian distributions with their mean and variance calculated from scan points falling into cells of a grid. Point to point matching approaches such as the approach presented in this paper, do not require the environment to be structured or contain predefined features.

Examples of point to point matching approaches are the following: iterative closest point (ICP), iterative matching range point (IMRP) and the popular iterative dual correspondence (IDC). Besl and Mac Kay [1992] proposed ICP, where for each point of the current scan, the point with the smallest Euclidean distance in the reference scan is selected. IMPR was proposed by Lu and Milios [1997], where corresponding points are selected by choosing a point which has the matching range from the center of the reference scan's coordinate system. IDC, also proposed by Lu and Milios [1997] combines ICP and IMRP by using the ICP to calculate translation and IMPR to calculate rotation. The mentioned point to point methods can find the correct pose of the current scan in one step provided the correct associations are chosen. Since the correct associations are unknown, several iterations are performed. Matching may not always converge to the correct pose, since they can get stuck in a local minima. Due to the applied association rules, matching points have to be searched across 2 scans, resulting in $O(n^2)$ complexity. If the search for corresponding points is reduced to a window with a constant angle, the computational complexity is $O(kn)$, where n is the number of scan points and k is proportional to the number of range readings per unit angle i.e. to the angular resolution of the scan. k is introduced to differentiate between increasing the number of scan points by increasing the field of view or the angular resolution of the laser range finder. However, it has been demonstrated [Nishino and Ikeuchi, 2002] that by using k-d trees one can expect to reduce the computational complexity of the correspondence search to $O(nlog(n))$ ($O(n^2)$ in the worst case). The mentioned approaches operate in a Cartesian coordinate frame and therefore do not take advantage of the native polar coordinate system of a laser scan. However as shown later in this paper, a scan matching algorithm working in the polar coordinate system of a laser scanner can eliminate the search for corresponding points thereby achieving $O(n)$ computational complexity for translation estimation. $O(n)$ computational complexity is achievable for orientation estimation if a limited orientation estimation accuracy is acceptable.

These point to point matching algorithms apply a so called projection filter [Gutmann, 2000] prior to matching. The objective of this filter is to remove those points from the reference and current scan not likely to have a corresponding point. The computational complexity of this filter is $O(n^2)$.

In recent years there have been a number of new point to point scan matching approaches. Minguez et al. [2006] have proposed a new distance metric used for selecting point associations and the calculation of the current scan pose. This metric promises to take rotation and translation better into consideration than the Euclidean (distance between points) distance metric of ICP. However, further work is necessary to choose an ad-hoc parameter combining translation and orientation difference in the proposed metric. Jensen and Siegwart [2004] and Montesano et al. [2005b] propose utilizing in their scan matching approaches the uncertainty in the laser measurements and in a prior pose estimate, during association search and pose estimation. However, the source of the prior pose estimate is often odometry for mobile robots. Unless the odometry parameters of a mobile robot are perfectly calibrated for all the surfaces the robot moves on, there will always be systematic errors in the odometry pose estimate which will bias the scan matching results. Further, if such a scan matching approach is used in EKF SLAM, one needs to estimate the correlation between the predicted pose and the measurement (i.e. the scan matching result) since they will not be independent. In other scan matching approaches the effects of odometry error are more limited since the pose estimate from odometry is often used only for initializing the matching, or not used at all. All of the mentioned recent approaches need to search for associations, and they are more complex than the simple polar scan matching approach proposed in this paper.

There are other scan matching approaches such as the method of Weiss and Puttkamer [1995]. Here for both reference and current scans, an angle-histogram of the orientation of line segments connecting consecutive points is generated. The orientation of the current scan with respect to the reference scan is obtained by finding the phase with the maximum cross correlation of the 2 angle histograms. The translation is found similarly by calculating x and y histograms, and calculating cross correlations. In scan matching, not all approaches use only that information in a scan, which describes where objects are located. Thrun et al. [2000] in their scan matching method utilize the idea, that free space in a scan is unlikely to be occupied in future scans. Surprisingly, Hough transform can also be used in scan matching as demonstrated in [Censi *et al.*, 2005; Censi, 2006].

Mapping with scan matching has been done for example by minimizing an energy function [Lu, 1995], using a combination of maximum likelihood with posterior estimation [Thrun *et al.*, 2000], using local registration and global correlation [Gutmann, 2000] and using FastSLAM [Hähnel *et al.*, 2003]. A Kalman filter implementation can be found in [Bosse *et al.*, 2004].

Laser scan matching approaches can not only be applied to laser scans but to measurements from an omnidirectional camera as well. In [Menegatti *et al.*, 2006], images of the floor are searched for color transitions to obtain range measurements which are matched to a prior map using Monte Carlo localization.

In this paper the Polar Scan Matching (PSM) approach is described which works in the laser scanner's polar coordinate system, therefore taking advantage of the structure of the laser measurements by eliminating the search for corresponding points. It is assumed that in the 2D laser measurements range readings are ordered by their bearings. Laser range measurements of current and reference scans are associated with each other using the matching bearing rule, which makes translation estimation of the PSM approach $O(n)$ complexity unlike IDC's $O(n^2)$ (or $O(kn)$ if the search window is limited to a constant angle). The orientation estimation's computational complexity is $O(n)$ if limited accuracy is acceptable, otherwise $O(kn)$. An $O(mn)$ complexity scan projection algorithm working in polar coordinates is also described in this paper. The variable m is defined as one more than the maximum number of objects occluding each other in the current scan viewed from the reference scan's pose. However this projection filter is of $O(n)$ complexity if no occlusions occur in the scan, therefore being more efficient than that of [Gutmann, 2000].

The rest of the paper is organized as follows; first scan preprocessing steps, followed by the PSM algorithm is described. Details of experimental results follow that include simulation, ground truth measurements and an implementation of SLAM. Finally conclusions and future work are presented.

The source code of PSM can be downloaded from www.irrc.monash.edu.au/adiosi.

2 Scan Matching

The laser scan matching method described in this section aligns the current scan with respect to the reference scan so that the sum of square range residuals is minimized. It is assumed that an initial pose of the current scan is given, expressed in the coordinate frame of the reference scan. Equations for the transformation of the current frame expressed in the world frame into the reference frame can be found in [Diosi and Kleeman, 2005]. The coordinate frame of a laser scan is centered at the point of rotation of the mirror of a laser scanner. The X axis or zero angle of the laser's Cartesian coordinate system coincides with the direction of the first reported range measurement. The current scan is described as $C = (x_c, y_c, \theta_c, \{r_{ci}, \phi_{ci}\}_{i=1}^n)$, where x_c, y_c, θ_c describe position and orientation, $\{r_{ci}, \phi_{ci}\}_{i=1}^n$ describe n range measurements r_{ci} at bearings ϕ_{ci}, expressed in the current scan's coordinate system. $\{r_{ci}, \phi_{ci}\}_{i=1}^n$ are ordered by the bearings in ascending order as they are received from a SICK laser scanner. The reference scan is described as $R = \{r_{ri}, \phi_{ri}\}_{i=1}^n$. If bearings where range measurements are taken are unchanged in current and reference scans then $\phi_{ri} = \phi_{ci}$. The scan matching works as follows (see fig. 1): after preprocessing the scans, scan projection followed by a translation estimation or orientation estimation are iterated. In the polar scan matching (PSM) of this paper, one orientation step is followed by one translation step. More details on these steps are given in the following subsections.

2.1 Scan Preprocessing

Preprocessing the current and the reference scans prior to matching helps to remove erroneous measurements, clutter or to group measurements of the same object to increase the accuracy and robustness of scan matching. In fig. 2 a laser scan is depicted in a Cartesian coordinate system. Corresponding raw range measurements are shown in fig. 3. Laser scans can have points which are not suitable for matching. Such points are:

- Points representing moving objects such as the legs of a person in fig. 2. Table and chair legs are such points as well, since they are less likely to be static in the

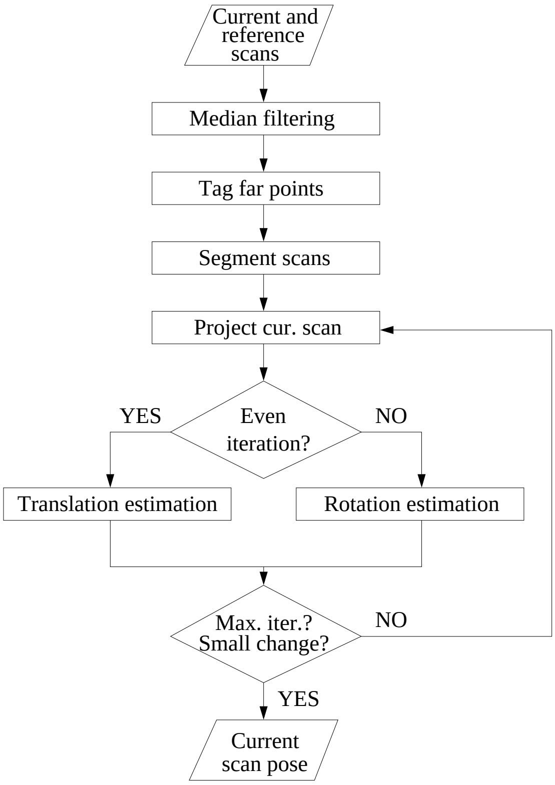

Figure 1: Scan matching algorithm.

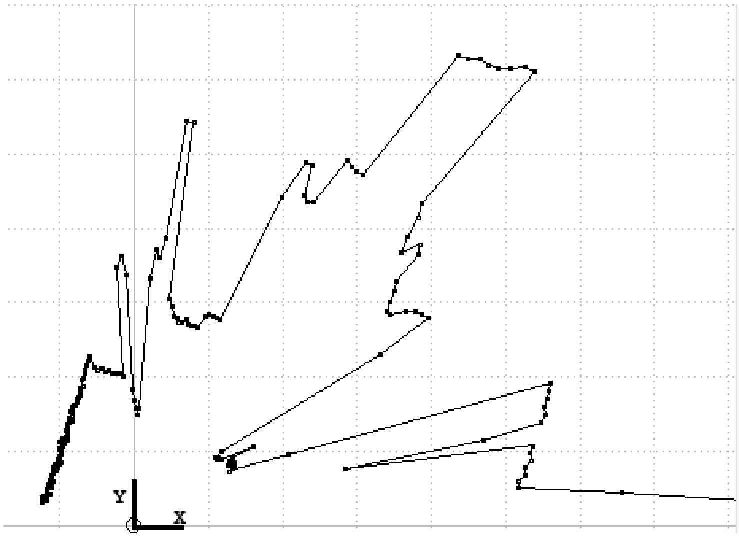

Figure 2: Laser scan in a Cartesian coordinate frame. Grid is 1m.

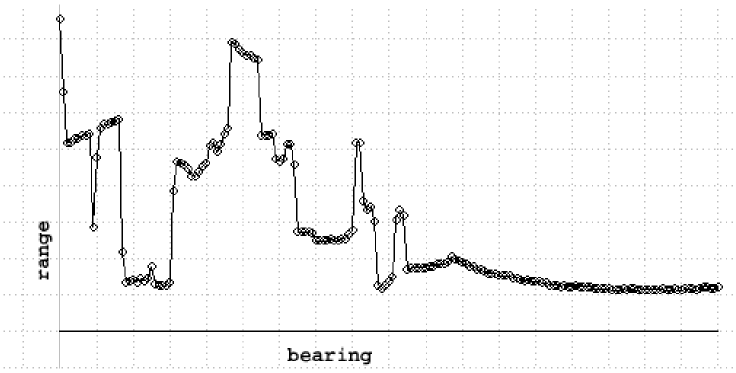

Figure 3: Scan of fig. 2 in the laser's polar coordinate frame. Horizontal grid size is 10°, vertical grid size is 1m.

long term.

- Mixed pixels. At range discontinuities laser scanners often generate measurements which are located in the free space between two objects [Ye and Borenstein, 2002].

- Measurements with maximum range. Such readings are returned, when there is no object within the range of the scanner. Some surfaces (for example clean clear glass) do not illuminate well and show a laser spot, therefore they can appear as measurements with maximum range.

In the implemented scan preprocessing first a median filter is used to replace outliers with suitable measurements as in [Gutmann, 2000]. With the application of a median filter to the range readings, objects such as chair and table legs are likely to be removed. The window size PM_MEDIAN_WINDOW is chosen based on the number of neighboring outliers one aims to replace. For example in [Gutmann, 2000], a window size of 5 for the median filter was found satisfactory since it can replace at most 2 neighborings outliers. This means, that chair or table legs are not removed by the scans if they are represented by more than 2 points.

After the application of a median filter all points further than a threshold PM_MAX_RANGE are tagged. These tagged points are used only in segmentation described next and not in scan matching. Range measurements larger than PM_MAX_RANGE are not used

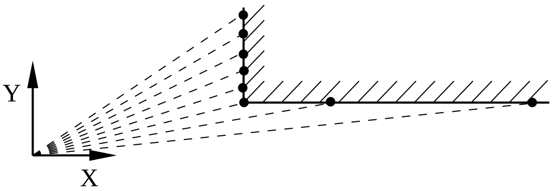

Figure 4: Only a proximity threshold for object segmentation is not enough because there can be large distances between points on walls nearly parallel with the laser beams.

in the scan matching because the distance between such measurements is large, which makes it hard to decide if they belong to the same object or not. Interpolating between two neighboring points belonging to 2 different objects can be a source of error. Artificially restricting the range of the sensor may introduce difficulties in large rooms with a lot of open space.

The choice of PM_MAX_RANGE depends on the maximum range and angular resolution of the sensor and on how scans are segmented. For example if neighboring points are sampled at 1° resolution and objects separated by 20cm are considered distinct, then there is no reason to use a range reading larger than 10m since the points are separated by at least 17cm.

The tagging of long range measurements is followed by the segmentation of the scan. Segmenting range measurements can have two advantages. The first advantage is that interpolation between 2 separate objects can be avoided if one knows that the objects are separate. Such interpolation is useful when one wants to know how a scan would look from a different location (scan projection). The second advantage is that if laser scans are segmented and the segments are tracked in consecutive scans then certain types of moving objects can be identified. Tracking moving objects as performed for example in [Montesano *et al.*, 2005a] can make scan matching more robust. However, motion tracking constitutes future work and is beyond the scope of this paper.

Two criteria are used in the segmentation process. According to the first criterion, a range reading, not differing more than PM_MAX_DIFF from the previous range reading, belongs to the same segment. This criterion fails to correctly segment out points which are for example on a wall oriented nearly parallel with the laser beams falling

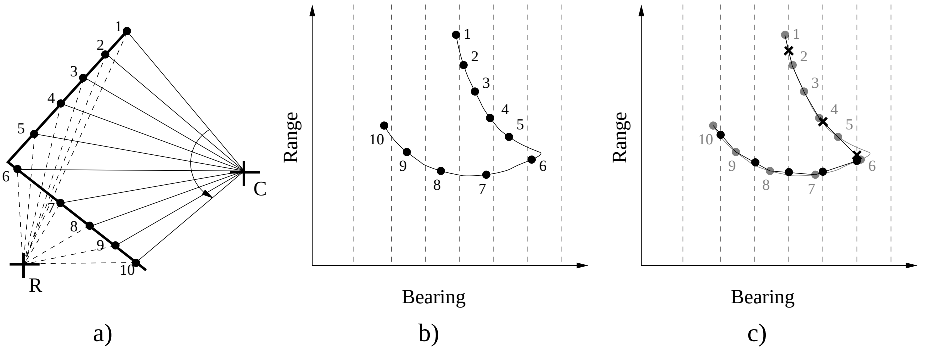

Figure 5: a) projection of measured points taken at C to location R. b) points projected to R shown in polar coordinates. Dashed lines represent bearings which the scanner would have sampled. c) Sampled visible points shown as black dots, sampled occluded points shown as “x”.

on it (see fig. 4). Therefore a second criterion is also applied according to which if 3 consecutive range readings lie approximately on the same line in the laser’s polar coordinate system, then they belong to the same segment. A mixed pixel can only connect two objects if the distance between the first object and the mixed pixel and the second object and the mixed pixel is less than PM_MAX_DIFF. Tagged range readings break segments as well.

Segments are assigned unique ID numbers, except 0, which is assigned to segments consisting of only one point. Segments assigned 0 are tagged, therefore they are not used in the scan matching process. Most of the mixed pixels get assigned 0.

The preprocessing steps are of $O(n)$ complexity. The values of the introduced constants are shown in section 3.

2.2 Scan Projection

An important step in scan matching is finding out how the current scan would look if it were taken from the reference position. For example in fig. 5, the current scan is taken at location C and the reference scan is taken at position R. The range and bearings of the points from point R (see fig. 5b) are calculated:

$$r'_{ci} = \sqrt{(r_{ci}\cos(\theta_c + \phi_{ci}) + x_c)^2 + (r_{ci}\sin(\theta_c + \phi_{ci}) + y_c)^2} \tag{1}$$

$$\phi'_{ci} = atan2(r_{ci}\sin(\theta_c + \phi_{ci}) + y_c,\ r_{ci}\cos(\theta_c + \phi_{ci}) + x_c) \tag{2}$$

where $atan2$ is the four quadrant version of $\arctan$.

In fig. 5b the dashed vertical lines represent sampling bearings (ϕ_{ri}) of the laser at position R in fig. 5a. Since the association rule is to match bearings of points, next ranges r''_{ci} at the reference scan bearings ϕ_{ri} are calculated using interpolation. The aim is to estimate what the laser scanner would measure from pose R. This resampling step consists of checking (r'_{ci}, ϕ'_{ci}) (i.e. 1,2,..10 in fig. 5b) of each segment if there are one or more sample bearings between 2 consecutive points (i.e. between 1 and 2 there is one, between 6 and 7 there are 2). By linear interpolation a range value is calculated for each sample bearing. If a range value is smaller than an already stored range value at the same bearing, then the stored range is overwritten with the new one to handle occlusion. As in [Lu and Milios, 1997] a new range value is tagged as invisible if the bearings of the 2 segment points are in decreasing order. The result of scan projection is shown in fig. 5c.

A pseudo code implementation of the described scan projection is shown in fig. 6. Unlike the equations in this paper, the indexes of vector elements in fig. 6 start from 0. The pseudo code on lines 00-07 transforms the current scan readings (ϕ_i, r_{ci}) into the reference scan's coordinate frame using the current frame pose (x_c, y_c, θ_c) expressed in the reference frame. Since the projected current scan (ϕ'_{ci}, r'_{ci}) is resampled next at the sample bearings ϕ_i of the reference scan, the data structures associated with the resampled current scan are also initialized. Status registers $tagged''_{ci}$ contain flags describing if resampled range readings r''_{ci} have been tagged or if they contain a range reading. All flags of the status registers are cleared except the flag PM_EMPTY which indicates that no range reading has been resampled into the particular position of the range array r''_c. Resampled current scan range readings r''_{ci} are initialized to a value which is larger than the maximum range of the laser scanner.

```
/**************Scan Projection*******************/
//Transform current measurements into reference frame
for i = 0 → number_of_points-1 do
    $x = r_{ci}\cos(\theta_c + \phi_i) + x_c$
    $y = r_{ci}\sin(\theta_c + \phi_i) + y_c$
    $r'_{ci} = \sqrt{x^2 + y^2}$
    $\phi'_{ci} = atan2(y, x)$
    $tagged''_{ci} = PM\_EMPTY$
    $r''_{ci} = LARGE\_VALUE$
//Given the projected measurements $(r'_{ci}, \phi'_{ci})$, calculate what would
//have been measured with the laser scanner at the reference pose.
for i = 1 → number_of_points-1 do
    if $segment_{ci} \neq 0$ & $segment_{ci} = segment_{ci-1}$
        !$tagged_{ci}$ & !$tagged_{ci-1}$ & $\phi'_{ci} > 0$ & $\phi'_{ci-1} \geq 0$ then
        if $\phi'_{ci} > \phi'_{ci-1}$ then //Is it visible?
            $occluded = false$
            $a_0 = \phi'_{ci-1}$
            $a_1 = \phi'_{ci}$
            $j_0 = ceil(\phi'_{ci-1}$/angular_resolution)
            $j_1 = floor(\phi'_{ci}$/angular_resolution)
            $r_0 = r'_{ci-1}$
            $r_1 = r'_{ci}$
        else
            $occluded = true$
            $a_0 = \phi'_{ci}$
            $a_1 = \phi'_{ci-1}$
            $j_0 = ceil(\phi'_{ci}$/angular_resolution)
            $j_1 = floor(\phi'_{ci-1}$/angular_resolution)
            $r_0 = r'_{ci}$
            $r_1 = r'_{ci-1}$
        while $j_0 \leq j_1$ do
            $r = \frac{r_1 - r_0}{a1 - a0}(j_0$ angular_resolution $- a_0) + r_0$
            if $j_0 \geq 0$ & $j_0 <$ number_of_points & $r''_{cj_0} > r$ then
                $r''_{cj_0} = r$
                $tagged''_{cj_0} \& = \sim PM\_EMPTY$
                if occluded then
                    $tagged''_{cj_0} | = PM\_OCCLUDED$
                else
                    $tagged''_{cj_0} \& = \sim PM\_OCCLUDED$
            $j_0 = j_0 + 1$
```

Figure 6: Scan projection pseudo code.

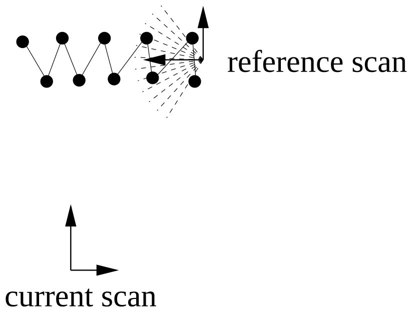

Figure 7: Example for the worst case scenario for scan projection.

The resampling of the projected current scan readings (ϕ'_{ci}, r'_{ci}) takes place on lines 10-38 in a loop which goes through neighboring pairs of (ϕ'_{ci}, r'_{ci}). Pairs of measurements are only resampled if they belong to the same segment (i.e. share the same ID) and none of them are tagged (lines 11-12). Next, on lines 13-28 the measurement pair is checked if it is viewed from behind by testing if $\phi'_{ci} > \phi'_{ci-1}$. Then depending on their order, ϕ'_{ci} and ϕ'_{ci-1} are converted into indexes j_0, j_1 into the resampled ranges array, so that $j_0 <= j_1$. In the conversion the angular resolution of the laser range finder is used. The conversion to indexes is done to simplify the following interpolation step where the resampled ranges r''_c are calculated in a while loop (lines 29-38) at index j_0 which is incremented until it reaches j_1. In the while loop first range r corresponding to j_0 is calculated using linear interpolation. Then if j_0 is within the bounds of the array r''_c and if r is smaller than the value already stored at r''_{cj_0} then the empty flag of $tagged''_{cj_0}$ is cleared and r''_{cj_0} is overwritten by r. This last step filters out those projected current scan readings which are occluded by other parts of the current scan. Finally the occluded flag of $tagged''_{cj_0}$ is cleared or set, depending on if ϕ'_{ci} was greater than ϕ'_{ci-1}, and j_0 is incremented.

The body of the while loop (lines 32-40) of the pseudo code is executed at most $2n$ times for scans with no occlusion, where n is the number of points. However it is easy to contrive a scenario where the inside of the while loop would execute at most n^2 times. For example fig. 7 depicts a situation where the noise in the current scan readings (drawn with connected circles) is large and the scan readings are aligned with the reference scan's frame so that most of the reference scan's laser beams go through in between the points of the current scan. In a such case for each pair of current scan points the while loop would execute almost n times resulting in a total number of executions between $2n$ and n^2. The computational complexity of this projection filter is $O(mn)$ where m is the maximum number of objects occluding each other in the current scan viewed from the reference scan's pose incremented by one. For example if there is no occlusion then m is 1. If there is at least one object which occludes another object, while the occluded object does not occlude any other object, then m is 2. If there are objects A, B and C where A occludes B and B occludes C then m is 3.

The scan projection filter described in [Gutmann, 2000] is of $O(n^2)$ complexity, because a double loop is employed to check for occlusion. That occlusion check consists of checking whether any current scan point in XY coordinates is obscured by any other pair of consecutive current or reference scan points. Since the scan projection implementation in fig. 6 is of $O(n)$ complexity when there are no occlusions in the current scan, it is reasonable to believe that under normal circumstances it is more efficient than that described in [Gutmann, 2000]. Due to its efficiency the projection filter of fig. 6 is applied in each iteration of the PSM scan matching algorithm.

The Cartesian projection filter in [Gutmann, 2000] removes all current scan points which are further than one meter from all reference scan points and vice versa. In PSM associated current and reference scan measurements with a residual larger than a preset threshold are ignored in the position estimation process and not in the projection filter. This eliminates the need for performing the computationally expensive removal of points without correspondence in the projection filter.

2.3 Translation Estimation

After scan projection, for each bearing ϕ_{ri} there is at most one r''_{ci} from the projected current scan and a corresponding r_{ri} from the reference scan. The aim is to find (x_c, y_c) which minimizes $\sum w_i(r_{ri} - r''_{ci})^2$, where w_i is a weight used to reduce the weighting[1] of bad matches. To minimize the weighted sum of square residuals linear regression

[1] In addition there is an implicit weighting of closer objects, since they cover a larger angle.

was applied to the linearized (1):

$$\Delta r_i \approx \frac{\partial r''_{ci}}{\partial x_c}\Delta x_c + \frac{\partial r''_{ci}}{\partial y_c}\Delta y_c = \cos(\phi_{ri})\Delta x_c + \sin(\phi_{ri})\Delta y_c \tag{3}$$

$\frac{\partial r''_{ci}}{\partial x_c} = \cos(\phi_{ri})$ has been derived from (1) the following way:

$$\begin{aligned} \frac{\partial r''_{ci}}{\partial x_c} &= \frac{1}{2}\frac{2(r_{cj}\cos(\theta_c+\phi_{cj})+x_c)}{\sqrt{(r_{cj}\cos(\theta_c+\phi_{cj})+x_c)^2+(r_{cj}\sin(\theta_c+\phi_{cj})+y_c)^2}} \\ &= \frac{(r_{cj}\cos(\theta_c+\phi_{cj})+x_c)}{r''_{ci}} = \frac{r''_{ci}\cos\phi_{ri}}{r''_{ci}} = \cos\phi_{ri} \end{aligned} \tag{4}$$

Where ϕ_{cj}, r_{cj} is a virtual, unprojected reading which would correspond to an uninterpolated ϕ_{ri}, r''_{ci}. The derivation of $\frac{\partial r''_{ci}}{\partial y_c}$ is analogous to the derivation of $\frac{\partial r''_{ci}}{\partial x_c}$.

If range differences between projected current range and reference range readings are modeled as

$$(\mathbf{r''_c} - \mathbf{r_r}) = \mathbf{H}\begin{bmatrix}\Delta x_c \\ \Delta y_c\end{bmatrix} + \mathbf{v} \tag{5}$$

where $\mathbf{v}$ is the noise vector and

$$\mathbf{H} = \begin{bmatrix} \frac{\partial r''_{c1}}{\partial x_c} & \frac{\partial r''_{c1}}{\partial y_c} \\ \frac{\partial r''_{c2}}{\partial x_c} & \frac{\partial r''_{c2}}{\partial y_c} \\ \cdots & \cdots \end{bmatrix}, \tag{6}$$

then the position correction $\Delta x_c,\ \Delta y_c$ of the current scan is calculated by minimizing the sum of weighted range residuals $\sum w_i(r_{ri} - r''_{ci})^2$ using the well known equation for weighted least squares [Kay, 1993]:

$$\begin{bmatrix}\Delta x_c \\ \Delta y_c\end{bmatrix} = (\mathbf{H^T W H})^{-1}\mathbf{H^T W}(\mathbf{r_r} - \mathbf{r''_c}) \tag{7}$$

where $\mathbf{r''_c}, \mathbf{r_r}$ are vectors containing r''_{ci} and r_{ri} and $\mathbf{W}$ is a diagonal matrix of weights. The elements of $\mathbf{W}$ are calculated according to the recommendations of Dudek and

Jenkin in [2000]:

$$w_i = 1 - \frac{d_i^m}{d_i^m + c^m} = \frac{c^m}{d_i^m + c^m} = \frac{PM\_C}{d_i^m + PM\_C} \tag{8}$$

where $d_i = r''_{ci} - r_{ri}$ is the error between projected current scan range measurements and reference scan range measurements and c is a constant. Equation (8) describes a sigmoid function with weight 1 at $d_i = 0$ and a small weight for large d_i. Parameter c determines where the sigmoid changes from 1 to 0, and m determines how quickly the sigmoid function changes from 1 to 0. In the experiments described in section 3 $m = 2$ was used. In [Dudek and Jenkin, 2000] (8) was used to weight the distance of a laser scan point to a line in a point-to-feature scan matching method.

To reduce the effects of association errors in the implementation of (7), only those visible measurements are taken into consideration which are not tagged (see section 2.1). In addition, the errors between reference and current scan range measurements have to be smaller than a preset threshold PM_MAX_ERROR to be included.

An example implementation for one step of the translation estimation can be seen in fig. 8. In the implementation first $\mathbf{H^T W H}$ and $\mathbf{H^T W} \Delta \mathbf{r}$ are calculated for untagged associated reference and current scan measurements, which are closer to each other than a threshold. Elements h1, h2 of the Jacobian matrix $\mathbf{H}$ on lines 05-06 have to be calculated only once, since ϕ_{ri} depends only on the type of laser scanner. Matrix $\mathbf{H^T W H}$ is inverted on lines 13-17 followed by the calculation of pose corrections. As one can see from fig. 8, translation estimation is of $O(n)$ complexity. The translation estimation step of IDC and ICP is of $O(n^2)$ complexity, or $O(kn)$ if a fixed angle search window is employed.

The equation used in other point-to-point scan matching methods which operate in XY coordinate systems such as ICP or IDC find the correct translation and rotation of the current scan in one step if the correct associations are given. The PSM approach, due to the use of linearization, requires multiple iterations. Since the correct associations are in general not known multiple iterations are typically necessary for the other methods as well. The PSM approach to translation estimation is most accurate if

```
/**************Polar Translation Estimation*****************/
//*Matrix multiplications for linearized least squares*
$hwr1 = hwr2 = hwh11 = hwh12 = hwh21 = hwh22 = 0$
**for** i = 0 → number_of_points-1 **do**
    $\Delta r = r_{ri} - r''_{ci}$
    **if** $!tagged''_{ci}$ & $!tagged_{ri}$ &$|\Delta r| < PM\_MAX\_ERROR$ **then**
        $w = \frac{PM\_C}{\Delta r^2 + PM\_C}$ //*weight calculation*
        $h1 = \cos\phi_{ri}$
        $h2 = \sin\phi_{ri}$
        $hwr1 = hwr1 + w * h1\Delta r$ //*calculating* $H^T W \Delta r$
        $hwr2 = hwr2 + w * h2\Delta r$
        $hwh11 = hwh11 + w * h1^2$ //*calculating* $H^T W H$
        $hwh12 = hwh12 + w * h1 * h2$
        $hwh21 = hwh21 + w * h1 * h2$
        $hwh22 = hwh22 + w * h2^2$
$D = hwh11 * hwh22 - hwh12 * hwh21$
$inv11 = \frac{hwh22}{D}$
$inv12 = -\frac{hwh12}{D}$
$inv21 = -\frac{hwh21}{D}$
$inv22 = \frac{hwh11}{D}$
$\Delta x = inv11 * hwr1 + inv12 * hwr2$
$\Delta y = inv21 * hwr1 + inv22 * hwr2$
$x_c = x_c + \Delta x$
$y_c = y_c + \Delta y$
```

Figure 8: Pseudo code for translation estimation in polar coordinates.

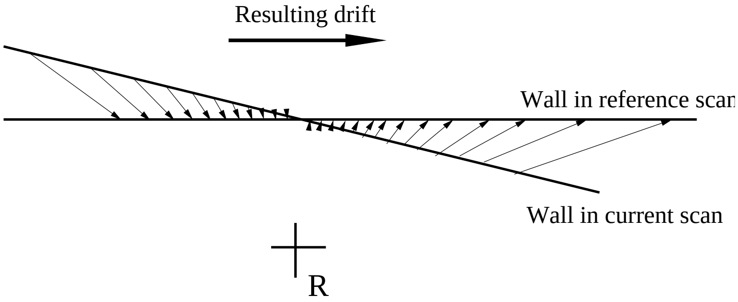

Figure 9: Cause of drift in for translation estimation in corridor like environments.

the correct orientation of the current scan is known. Estimating the orientation of the current scan is described in section 2.4.

A negative property of this translation estimation approach is apparent when matching scans which were taken of long featureless corridors - the position error along the corridor can drift. In fig. 9 the reference and current scan contain only a wall. The associations are depicted with an arrow pointing from the current scan point to the reference scan point. The direction of the arrows coincide with the corresponding Jacobians which project into the x and y corrections. From fig. 9 it can be observed, that all the arrows have a positive x component, therefore the translation correction will drift to the right.

There are two reasons why polar scan matching estimates translation separately from orientation. First reason: if the partial derivatives $\frac{\partial r''_{ci}}{\partial \theta_c} = y_c \cos\phi_{ri} - x_c \sin\phi_{ri}$ are appended to matrix $\mathbf{H}$ (6), the matrix $\mathbf{H^T W H}$ can become ill-conditioned and the estimation process can diverge. The cause of ill-conditioning lies in the structure of $\mathbf{H}$:

$$\mathbf{H} = \begin{bmatrix} \vdots & \vdots & \vdots \\ \cos\phi_{ri} & \sin\phi_{ri} & y_c \cos\phi_{ri} - x_c \sin\phi_{ri} \\ \vdots & \vdots & \vdots \end{bmatrix}, \tag{9}$$

where two columns contain small numbers in the range of $\langle -1, 1\rangle$ and the third column contains potentially large numbers depending on the value of x_c and y_c. As an example let us assume that $x_c = 100cm,\ y_c = 100cm,\ \phi_{ri} = 0°, 1°, 2°, ..., 180°$ and $\mathbf{W}$ is a diagonal matrix with 1's on the diagonal. Then the largest eigenvalue of $\mathbf{H^T W H}$ is about 2×10^6 and the smallest eigenvalue is about 3×10^{-33} which means the matrix $\mathbf{H^T W H}$ is ill-conditioned and will likely cause numerical instability. On the other hand if x_c and y_c are 0, then the right column of $\mathbf{H}$ will consist of 0's and $\mathbf{H^T W H}$ will have 0 determinant and will not have an inverse which is necessary for the computation of (7). Even if x_c and y_c are small, and the process converges, the convergence speed is slow. The second reason why polar scan matching estimates translation separately from orientation is that as shown later, it is possible to accurately estimate the orientation in one step if the error in the current scan position is small.

If uniform weights were used, and all measurements were used in each scan matching, then matrix $(\mathbf{H^T W H})$ is a constant matrix and as such it has to be calculated only once.

It is interesting to investigate how the matching bearing association rule performs with the pose estimation equations described in Lu and Milios [1997]. The details are given next.

2.3.1 Pose Estimation in Cartesian Frame

Lu and Milios in [1997] minimize the sum of square distance between current and actual scan points. To increase robustness it is recommended in [Gutmann, 2000], that only the best 80% of matches take part in the estimation process. Here instead of sorting the matches, each match is weighted based on its "goodness", as in the previous subsection. The original objective function in [Lu and Milios, 1997] expressed using the notation used in this paper is:

$$E = \sum_{i=1}^{n} (x''_{ci} \cos\Delta\theta_c - y''_{ci} \sin\Delta\theta_c + \Delta x_c - x_{ri})^2 + (x''_{ci} \sin\Delta\theta_c + y''_{ci} \cos\Delta\theta_c + \Delta y_c - y_{ri})^2 \tag{10}$$

Where (x''_{ci}, y''_{ci}) correspond to the projected and interpolated current scan's (ϕ_{ri}, r''_{ci}) in Cartesian coordinate frame. (x_{ri}, y_{ri}) corresponds to (ϕ_{ri}, r''_{ri}) of the reference scan.

The weighted version used in this paper:

$$E = \sum_{i=1}^{n} w_i \left[(x''_{ci} \cos \Delta\theta_c - y''_{ci} \sin \Delta\theta_c + \Delta x_c - x_{ri})^2 + (x''_{ci} \sin \Delta\theta_c + y''_{ci} \cos \Delta\theta_c + \Delta y_c - y_{ri})^2 \right] \tag{11}$$

Since (x_{ci}, y_{ci}) belong to the same bearing as (x_{ri}, y_{ri}), (11) is equivalent to the sum of weighted square range residuals $\sum w_i (r_{ri} - r''_{ci})^2$ used in the previous subsection. A solution to (11) can be obtained by solving $\frac{\partial E}{\partial x_c} = 0,\ \frac{\partial E}{\partial y_c} = 0$ and $\frac{\partial E}{\partial \theta_c} = 0$:

$$\begin{aligned}
\Delta\theta_c &= atan2 \left(\bar{x}_r \bar{y}''_c - \bar{x}''_c \bar{y}_r + W(S_{y_r x''_c} - S_{x_r y''_c}), -\bar{y}_r \bar{y}''_c - \bar{x}''_c \bar{x}_r + W(S_{x_r x''_c} - S_{y_r y''_c}) \right) && (12) \\
\Delta x_c &= \frac{\bar{x}_r - \bar{x}''_c \cos \Delta\theta_c + \bar{y}''_c \sin \Delta\theta_c}{W} && (13) \\
\Delta y_c &= \frac{\bar{y}_r - \bar{x}''_c \sin \Delta\theta_c - \bar{y}''_c \cos \Delta\theta_c}{W} && (14)
\end{aligned}$$

where

$$\begin{aligned}
\bar{x}_r &= \sum w_i x_{ri}, & \bar{y}_r &= \sum w_i y_{ri} \\
\bar{x}''_c &= \sum w_i x''_{ci}, & \bar{y}_c &= \sum w_i y''_{ci} \\
S_{x_r y''_c} &= \sum w_i x_{ri} y''_{ci}, & S_{x''_c y_r} &= \sum w_i x''_{ci} y_{ri} \\
S_{x_r x''_c} &= \sum w_i x_{ri} x''_{ci}, & S_{y''_c y_r} &= \sum w_i y''_{ci} y_{ri} \\
W &= \sum w_i
\end{aligned} \tag{15}$$

Even though the objective function here is equivalent to the objective function in the previous subsection, the solutions are not equivalent. In the previous subsection, one iteration returns an approximate solution for x_c, y_c. Linearization was necessary due to the square root in (1). Here on the other hand a solution is calculated without linearization and without the need for multiple iterations (assuming known associations), which contains θ_c and not just x_c, y_c. In experiments it was found that if only (12)–(14) are used to estimate pose, then the convergence speed is unsatisfactory, and the estimation process is more likely to get stuck in a local minima. Therefore just as in the previous subsection, it is best to interleave the described way of estimating x_c, y_c, θ_c with the orientation estimation described in the following subsection.

The advantage of using (12)–(14) for calculating a solution of $\sum w_i (r_{ri} - r''_{ci})^2$

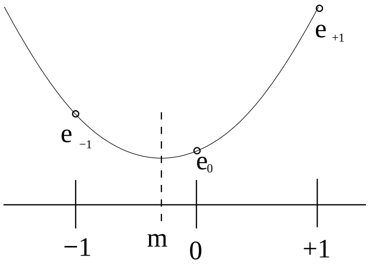

Figure 10: Orientation estimate improvement by interpolation.

in one step opposed to the multiple iteration needed when using (7) is not important since the unknown associations of the reference and current scan points anyway require an iterative pose estimation process. From now on using (12)–(14) together with the orientation estimation approach described next will be called PSM-C.

2.4 Orientation Estimation

Change of orientation of the current scan is represented in a polar coordinate system by a left or right shift of the range measurements. Therefore assuming that the correct location of the current scan is known and the reference and current scans contain measurements of the same static objects, the correct orientation of the current scan can be found by shifting the projected current scan (r''_{ci}, ϕ_{ri}) until it covers the reference scan. A $\pm 20^\circ$ shift was implemented at 1° intervals of the projected current scan, and for each shift angle the average absolute range residual is calculated. Orientation correction is estimated by fitting a parabola to the 3 closest points to the smallest average absolute error, and calculating the abscissa of the minimum.

The calculation of the abscissa of the minimum is performed as follows. Assume that the 3 points of the error function are $(-1, e_{-1})$, $(0, e_0)$ and $(+1, e_{+1})$ (see fig. 10). Then the abscissa m of the minimum e_m of the parabola described as $e = at^2 + bt + c$ is sought. Given the equation of the parabola, the abscissa of the minimum can be found at:

$$\frac{\partial e}{\partial t} = 0 = 2am + b = 0 \Rightarrow m = -\frac{b}{2a} \tag{16}$$

To find a, b let us substitute the 3 known points into the equation of the parabola:

$$a - b + c = e_{-1} \tag{17}$$

$$c = e_0 \tag{18}$$

$$a + b + c = e_{+1} \tag{19}$$

By substituting (18) into (17) and (19), and adding (17) and (19), one gets:

$$2a + 2e_0 = e_{-1} + e_{+1} \Rightarrow a = \frac{e_{-1} + e_{+1} - 2e_0}{2} \tag{20}$$

Similarly b can be calculated by subtracting (17) from (19):

$$2b = e_{+1} + e_{-1} \Rightarrow b = \frac{e_{+1} - e_{-1}}{2} \tag{21}$$

Then the abscissa of the minimum is:

$$m = -\frac{b}{2a} = -\frac{\frac{e_{+1}-e_{-1}}{2}}{2\frac{e_{-1}+e_{+1}-2e_0}{2}} = \frac{e_{+1} - e_{-1}}{2(2e_0 - e_{-1} - e_{+1})} \tag{22}$$

Assuming the orientation correction corresponding to 0 in fig. 10 is $\Delta\theta_1$, the distance between 0 and 1 in fig. 10 is $\Delta\phi$, then the estimated orientation correction will be

$$\Delta\theta_c = \Delta\theta_1 + m\Delta\phi \tag{23}$$

A simple pseudo code implementation of the orientation estimation is shown in fig. 11. In fig. 11 on lines 01-18 average absolute range residuals are calculated while shifting the reference range readings left and right by Δi. The value of Δi changes in the range of ±PM_SEARCH_WINDOW. The value of PM_SEARCH_WINDOW is chosen so, that the range of shift is around $\pm 20°$. On lines 03-08 those indexes into the current range readings array are calculated which overlap with the shifted reference range array. In a for loop average absolute range residuals are calculated only for untagged range readings. The average range residuals for the corresponding shift values are then stored in $error_k$ and in β_k. Then the minimum error and the corresponding shift value is found on lines 20-23, which is improved by fitting a parabola on lines 24-25. $\Delta\phi$ on line 25 is the angle corresponding to changes of Δi.

The computational complexity of this orientation estimation approach depends on how the increments of Δi are chosen. If the reference scan is shifted by constant increments for example by 1° then the computational complexity is $O(n)$. The justifications for using constant increments, opposed to the smallest possible increment which is the angular resolution of the scan are the following:

- The orientation estimates are improved by quadratic interpolation.
- When performing scan matching in real environments the error in orientation due to fixed Δi increments will likely to be much smaller than errors caused by incorrect associations.

If the increments of Δi are chosen to be equal to the bearing resolution of the scans, then assuming a constant size of search window in angles, the orientation estimation will be of $O(kn)$ complexity, where k is proportional to the number of range measurements per unit angle, i.e. to the angular resolution of the scan.

The last possibility discussed here in the choice of the increments of Δi is when one starts from a coarse increment of Δi and iteratively reduce Δi together with the size of the search window. In this case the computational complexity of $O(n \log n)$ may be achieved.

3 Experimental Results

The results of 4 experiments are presented where the performance of PSM, PSM-C (polar scan matching using Cartesian coordinates) and an implementation of ICP are compared. In the first experiment simulated laser scans are matched and evaluated. The remaining experiments use a SICK LMS 200 laser range finder at a 1° bearing resolution in indoor environments. In the second experiment, laser scan measurements are matched at 10 different scenes by positioning the laser manually in known relative

```
/**************Orientation estimation*****************/
$k = 0$
for $\Delta i = -PM\_SEARCH\_WINDOW \rightarrow +PM\_SEARCH\_WINDOW$ do
    $n = 0, e = 0$
    if $\Delta i <= 0$ then
        $min\_i = -\Delta i$
        $max\_i =$ number_of_points
    else
        $min\_i = 0$
        $max\_i =$ number_of_points$-\Delta i$
    for i = $min\_i \rightarrow max\_i - 1$ do
        if $!tagged''_{ci}$ & $!tagged_{ri+\Delta i}$ then
            $e = e + |r''_{ci} - r_{ri+\Delta i}|$
            $n = n + 1$
    if $n > 0$ then
        $error_k = \frac{e}{n}$
    else
        $error_k = LARGE\_VALUE$
    $\beta_k = \Delta i$
    $k = k + 1$
$e\_min = LARGE\_VALUE$
for i = 0 → k-1 do
    if $error_i < e\_min$ then
        $e\_min = LARGE\_VALUE$
        $i\_min = i$
$m = \frac{error_{i\_min+1} - error_{i\_min-1}}{2(2error_{i\_min} - error_{i\_min-1} - error_{i\_min+1})}$
$\theta_c = \theta_c + (\beta_{i\_min} + m)\Delta\phi$
```

Figure 11: Pseudo code for orientation estimation in polar coordinates.

PM_MAX_ERROR	100cm
PM_MAX_RANGE	1000cm
PM_MAX_ITER	30
PM_MIN_VALID_POINTS	40
PM_MAX_DIFF	20cm
PM_SEARCH_WINDOW	20°
PM_MEDIAN_WINDOW	5
PM_C	$(70cm)^2$ reduced to $(10cm)^2$ after 10 iterations

Table 1: Parameters used in scan matching during the experiment.

poses and the results are compared with the known relative poses. In the third experiment, the areas of convergence for particular pairs of scans are investigated. The scan matching algorithms are evaluated in a SLAM experiment in the fourth experiment. The parameters used in all scan matching experiments are shown in tab. 1.

Every scan matching variant was stopped and divergence declared if the number of matches sank below PM_MIN_VALID_POINTS. The terminating condition for PSM and PSM-C was that either in 4 consecutive iterations

$$\epsilon = |\Delta x_c[cm]| + |\Delta y_c[cm]| + |\Delta \theta_c[^\circ]| \tag{24}$$

was smaller than 1 or the maximum number of iterations PM_MAX_ITER has been reached. The need for a hard limit on the number of iterations is necessary, since PSM position estimate might drift along corridors. Another reason for a hard limit is to prevent the possibility of PSM and PSM-C entering a limit cycle. In the case of ICP, the terminating condition had to be chosen as $\epsilon < 0.1$, because of the low convergence speed of ICP. In the case of $\epsilon < 1$, ICP often terminated with a too large error. Due to the slow convergence speed, the maximum number of iterations was chosen as 60 for ICP, which is twice as much as that for PSM.

In PSM one position estimated step was followed by one orientation estimation step. These 2 steps are considered as 2 iterations. In PSM-C 3 pose estimation steps are followed by 1 orientation step. These 4 steps were considered as 4 iterations. This way of counting iterations is different to [Lu and Milios, 1997] where one position estimation step followed by an orientation estimation step was considered as one iteration for IDC.

In the following results, all the run times were measured on a 900MHz Celeron laptop.

3.1 ICP Implementation

In the ICP implementation, the same preprocessing steps are applied to the range readings of the reference and current scan as in PSM. Then in each iteration the projection of the current scan follows similarly to [Lu and Milios, 1997]. First each current scan point is transformed into the reference scan's Cartesian coordinate system. Current scan points are then checked if they are visible from the reference position by checking the order of points. This is followed by checking if two neighboring (in a bearing sense) reference or current scan points occlude the current scan point being checked. Occluded current scan points are then removed, if they are at least one meter further back than their interpolated reference counterparts. Current scan points not in the field of view of the laser at the reference location are removed as well. None of the reference scan points are removed like in the projection filter in [Gutmann, 2000]. Reference scan points are not searched in this projection filter implementation, therefore this implementation is faster than of [Gutmann, 2000].

After scan projection, the implementation of the closest point association rule follows. For each remaining current scan point the closest reference scan point is sought in a $\pm 20^\circ$ window. Then the worst 20% percent of associations are found and excluded. From the remaining associated point pairs pose corrections are calculated using equations from [Lu and Milios, 1997] and the current pose is updated.

The ICP algorithm is simpler than that described in [Lu and Milios, 1997] because the search window size is not reduced exponentially with the number of iterations. However the window is not reduced in the PSM and PSM-C orientation search either, therefore the comparison is fair. Unlike in [Lu and Milios, 1997] projection of the current scan with occlusion testing has been implemented without expensive searches and therefore it has been included at the beginning of each iteration. Performing an occlusion check in each iteration opposed to once at the beginning can increase the

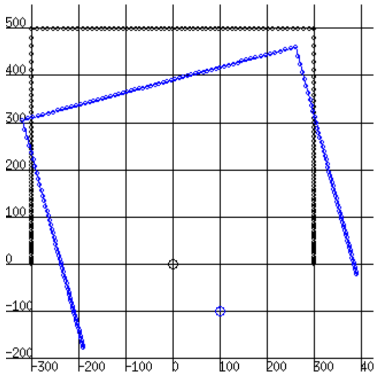

Figure 12: Current and reference scan prior to matching. Grid size in 1x1m.

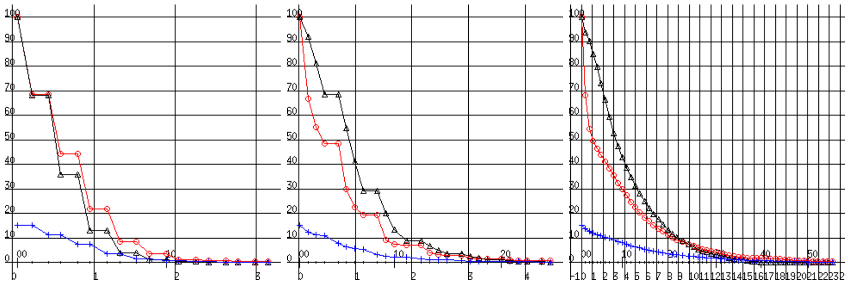

a) b) c)

Figure 13: Evolution of x (circles), y (triangles) and orientation (crosses) error expressed in $[cm]$ and $[^\circ]$, respectively of PSM, PSM-C and ICP in the simulated experiment. Grid size is 1ms x 10cm and 1ms x 10°, respectively. Iterations are marked with small vertical lines on the horizontal axis. Each 10-th iteration is marked with a longer vertical line.

accuracy of the results in the case of large initial errors where many visible points may be removed incorrectly or many invisible points are left in the scan incorrectly.

3.2 Simulated Room

Figure 12 shows two simulated scans of a room. The scans are identical, except the x and y position of the current scan was altered by 100cm. Orientation was altered by 15°. Figure 13 shows the evolution of errors of scan matching using PSM, PSM-C and ICP. The final errors can be see in tab. 2.

From fig. 13 and tab. 2 one can observe that all tree algorithms achieved approximately the same final pose error. PSM-C achieved slightly less accuracy than ICP and

	iterations	time [ms]	$\lvert\Delta x\rvert$[cm]	$\lvert\Delta y\rvert$[cm]	$\lvert\Delta\theta\rvert$ [°]
PSM	17	3.1	0.4	0.005	0.16
PSM-C	26	4.43	0.61	0.2	0.2
ICP	55	23.29	0.39	0.005	0.15

Table 2: Scan matching results of the simulated room.

PSM. Table 2 indicates that the terminating conditions of all scan matching approaches are set to achieve the same accuracy under ideal conditions such as the shown simulated scan. From tab. 2 one can also see that ICP needed more than three times as many iterations as PSM to reach the same error. The ICP took more than 7 times longer to converge than PSM.

All three scan matching algorithms were able to approach zero pose error in the simulated room experiment if the terminating condition ϵ in (24) was lowered accordingly. Lowering ϵ too much when matching real scans may unnecessarily increase the runtime without reducing the final pose error which may be caused by wrong associations.

3.3 Ground Truth Experiment

To determine how the polar scan matching algorithm variants cope with different types of environments, an experiment with ground truth information was conducted. On 4 corners of a 60x90cm plastic sheet, 4 Sick LMS 200 laser scanner outlines were drawn with different orientations. This sheet was then placed into different scenes ranging from rooms with different degrees of clutter to corridors. At each scene, laser scans were recorded from all 4 corners of the sheet, and matched against each other with initial positions and orientations deliberately set to 0 in the iterative procedure. The combinations of scans taken at corners which take part in the scan matching are shown in tab. 3. Ground truth values have been determined by measuring the left bottom corners of each outline with respect to an accurate grid printed on the plastic sheet. The carefully determined ground truth values for current scan poses in reference scan frames which also correspond to the initial errors are also displayed in tab. 3. From tab. 3 one can see, that the initial errors were up to 80cm displacement and up to 27°

orientation. During the experiments the environment remained static.

A matched current and reference scan from each scene is displayed in fig. 14 for PSM, fig. 16 for PSM-C and fig. 18 for ICP. The evolution of pose error is shown in fig. 15 for PSM, fig. 17 for PSM-C and fig. 19 for ICP. The displayed scans have all undergone median filtering. Only results for match 3 for each scene are displayed because match 3 contains a large initial error in displacement (71cm) and a large initial error in orientation ($-27°$) as can be seen from tab. 3. Absolute residual between ground truth and match results together with number of iterations and runtime are shown in tables 5–7. There are 6 error vectors corresponding to each match for each scene. In tab. 5 “ERROR” denotes a situation, when scan matching stopped due to the lack of corresponding points and divergence was declared.

Scene 0 is a room with a small degree of clutter. Current and reference scans were quite similar, and the matching results are good. Scene 1 is in a more cluttered room where laser scans from different locations look different as one can see in fig. 14. The reason why the current scan differs from the reference scan so much is not clear. Perhaps the objects in the room were not uniform in the vertical direction and the laser beam is not a small spot or the laser was slightly tilted. The results for scene 1 (see tables 5–7, row 1) are not good for any of the 3 implementations, but they are still usable for example in a Kalman filter with an appropriate error estimate. In scene 2 the sheet was placed in front of a door to a corridor. The results are excellent. Scene 3 is a corridor without features. While the orientation error and the error in the cross corridor direction were quite small, the along corridor errors are large. PSM has the largest along corridor error of all, since the solution can drift in the direction of the corridor. With a proper error model (small orientation and cross corridor error, large along corridor error) the results are still useful when used with a Kalman filter. Scenes 4, 5 and 6 are similar to 3. In scene 4 PSM diverged once. When observing the results for 4, 5 and 6 in fig. 14, there are phantom readings appearing at the corridor ends, even though the real corridor ends were 30 meters away. The likely reason for the phantom readings is a slight tilt of the laser beams causing readings from the floor to be obtained. Scene 7 is situated on the border of a room and a corridor. The results are good for all 3

match number	ref. scan recorded at corner	current scan recorded at corner	x [cm]	y [cm]	θ [°]
0	0	1	39.41	2.12	13
1	0	2	2.02	66.55	-14
2	0	3	38.84	66.99	12
3	1	2	-21.94	68.33	-27
4	1	3	14.04	68.33	-1
5	2	3	35.62	9.33	26

Table 3: Combinations of scans taken at different corners (numbered 0-3) of the plastic sheet for the ground truth experiment. These combinations marked as match number 0-5 were used for each scene. The shown poses of current scans with respect to reference scans correspond to the initial errors in the ground truth experiment.

	iterations	time [ms]	orientation err. [°]	displacement err. [cm]
PSM	18.57	3.35	0.86	3.8
PSM-C	15.78	2.67	0.92	3.8
ICP	42.57	19.54	3.65	10.8

Table 4: Summary of average scan matching results in the ground truth experiment.

scan matching methods. Scenes 8 and 9 were situated in a room. The results are quite good except of two matches of ICP when ICP converged to local minima.

To compare the 3 scan matching approaches average of errors, number of iterations and run times were calculated and shown in tab. 4. Average absolute orientation error, iteration and run time were calculated for all scenes except for the scenes 4, 5, 6 with the large phantom objects. In the average absolute displacement error calculation, all corridor like environments (3, 4, 5, 6) were left out, due to the large along corridor errors.

In the ground truth experiment, the implemented PSM and PSM-C clearly outperformed the implemented ICP. According to tab. 4 the performance of PSM and PSM-C are almost the same, with PSM being slightly more accurate but slower.

3.4 Convergence Map

The purpose of this experiment is to find those initial poses from which scan matching converges to an acceptable solution. Ideally one varies the initial position and orientation of the current scan in a systematic way and observes if the found solution is close

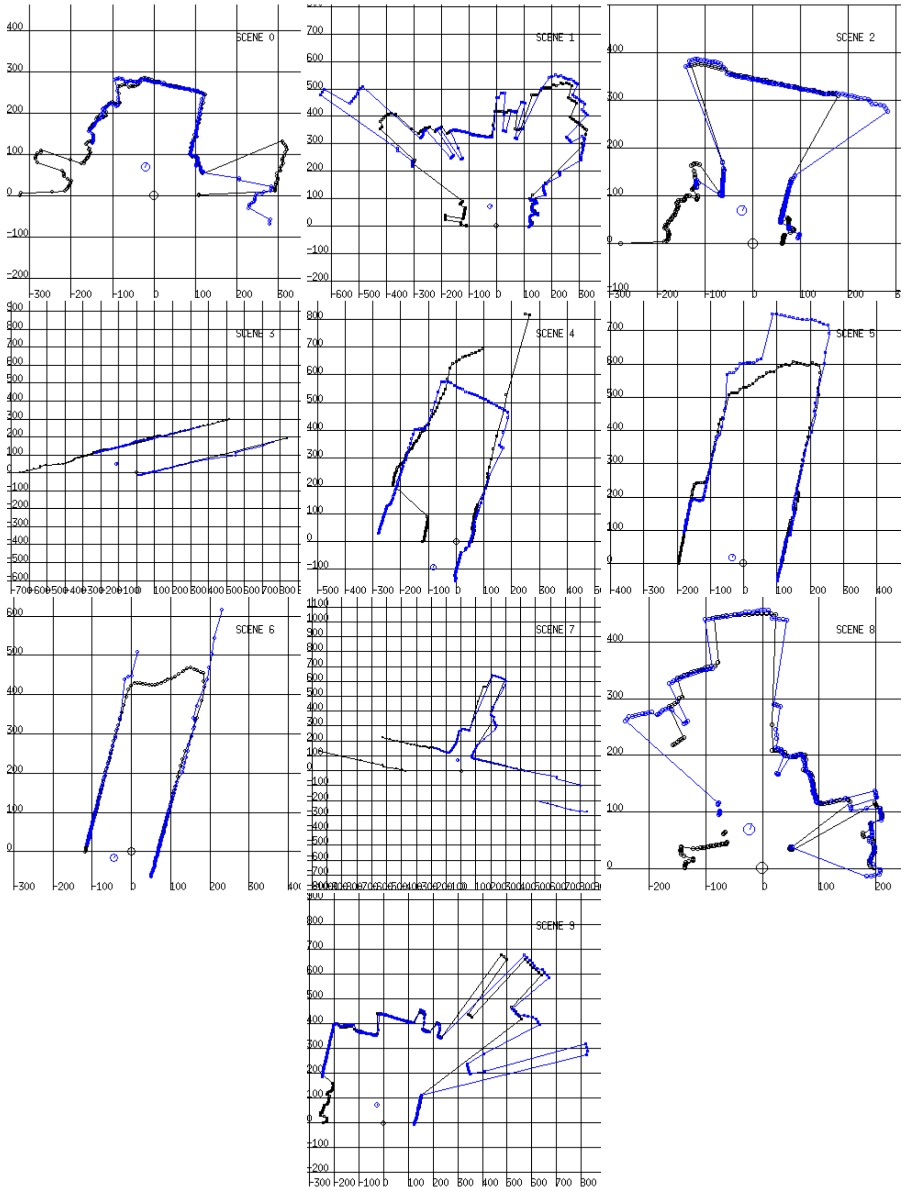

Figure 14: Scan match result for each scene for match number 3 in the experiment with ground truth using PSM.

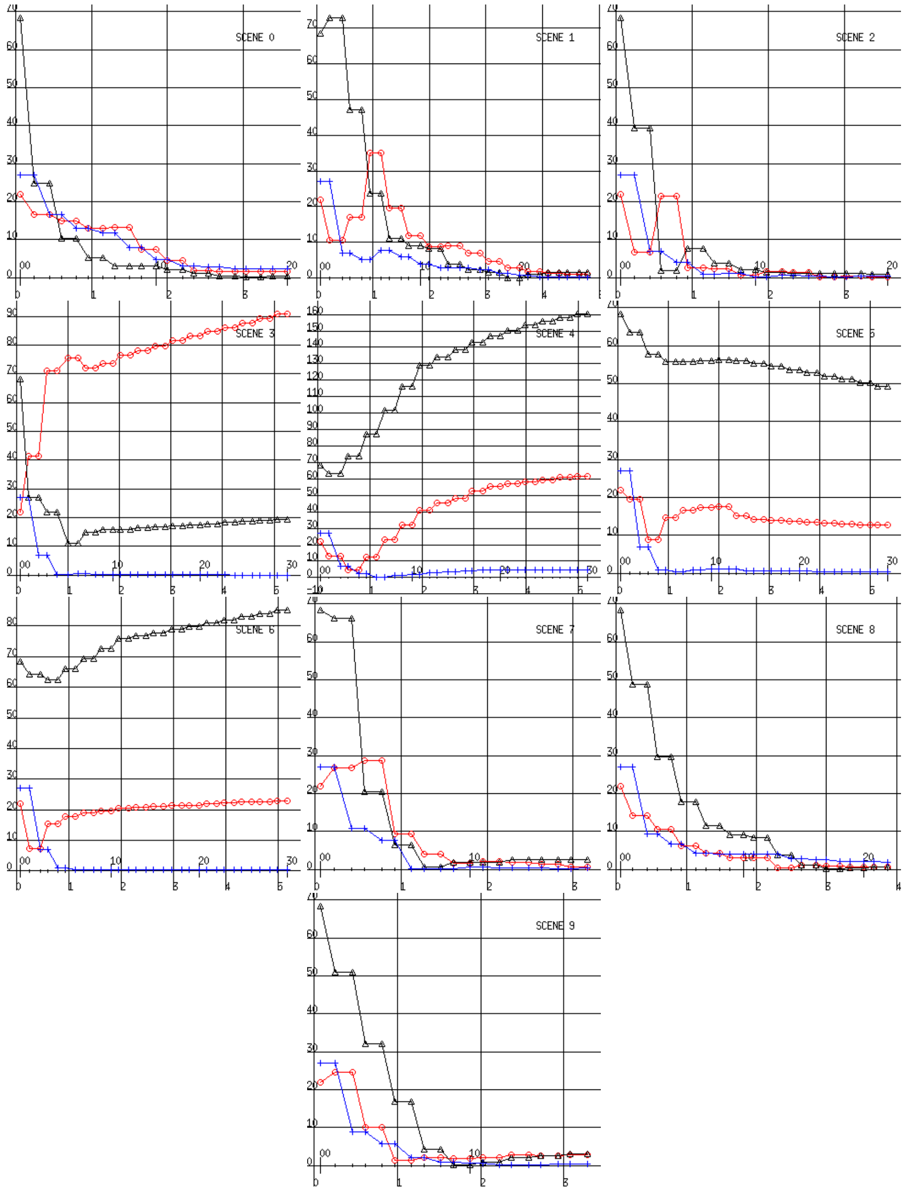

Figure 15: Match 3 scan match error evolution for each scene in the experiment with ground truth using PSM. Error in x (circles), y (triangles) and orientation (crosses) are expressed in $[cm]$ and $[^\circ]$, respectively. Grid size is 1ms x 10cm and 1ms x 10°, respectively. Iterations are marked with small vertical lines on the horizontal axis. Each 10-th iteration is marked with a longer vertical line.

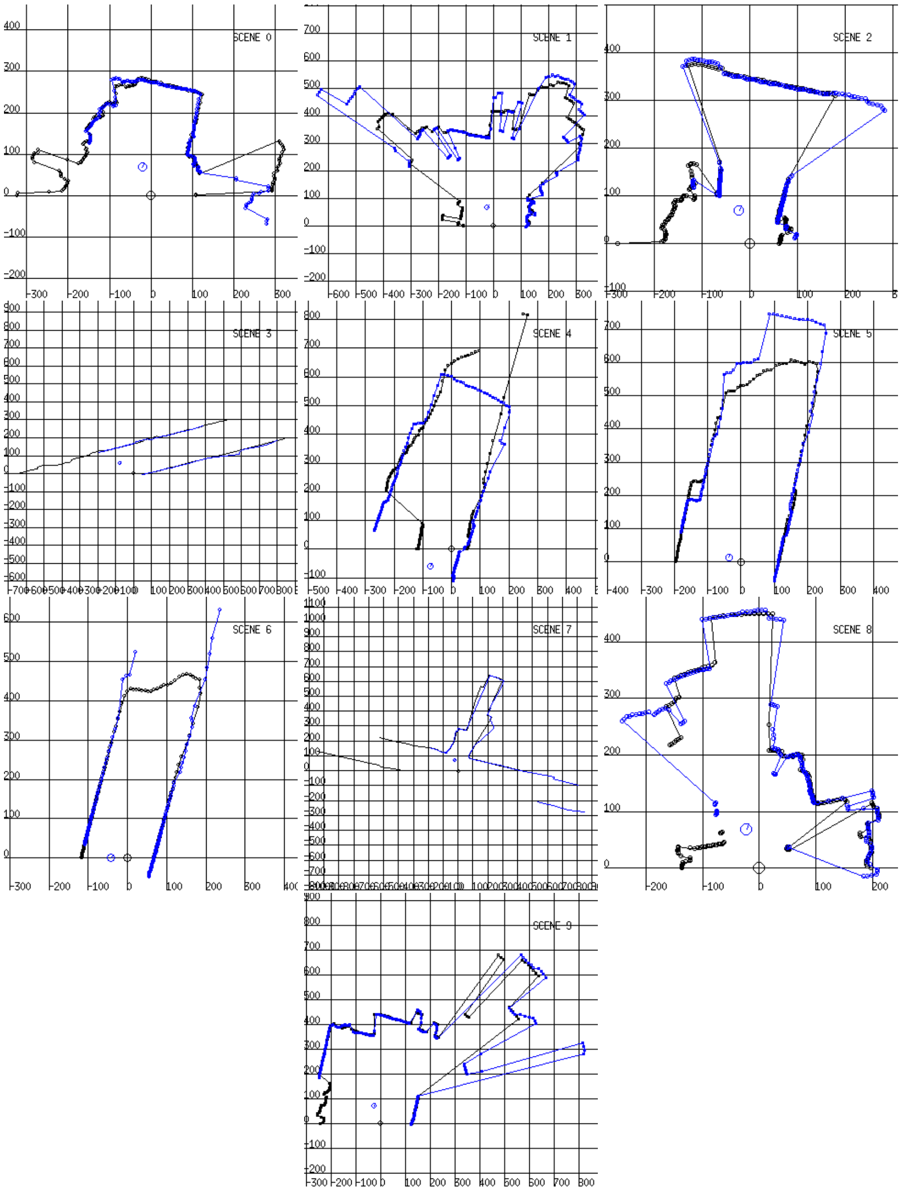

Figure 16: Scan match result for each scene for match number 3 in the experiment with ground truth using PSM-C.

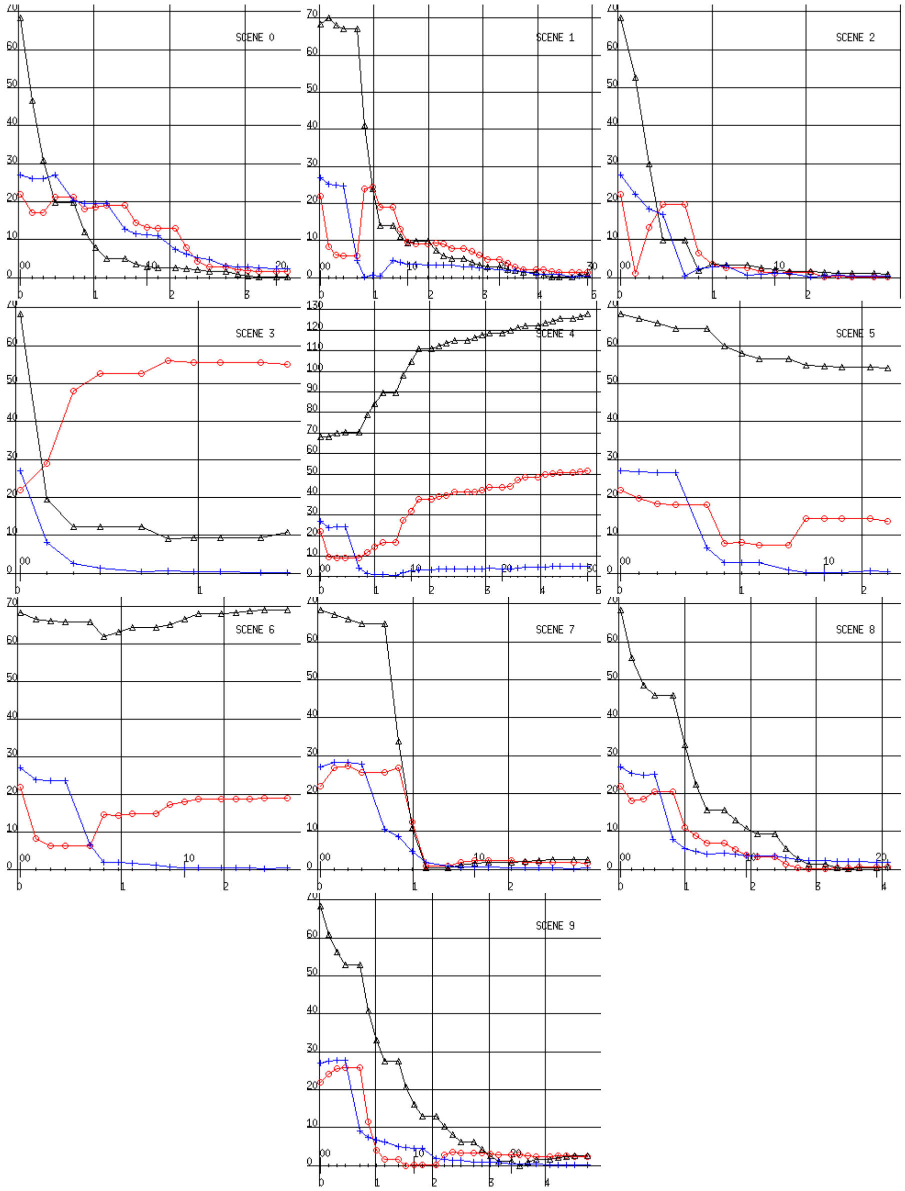

Figure 17: Match 3 scan match error evolution for each scene in the experiment with ground truth using PSM-C. Error in x (circles), y (triangles) and orientation (crosses) are expressed in $[cm]$ and $[°]$, respectively. Grid size is 1ms x 10cm and 1ms x 10°, respectively. Iterations are marked with small vertical lines on the horizontal axis. Each 10-th iteration is marked with a longer vertical line.

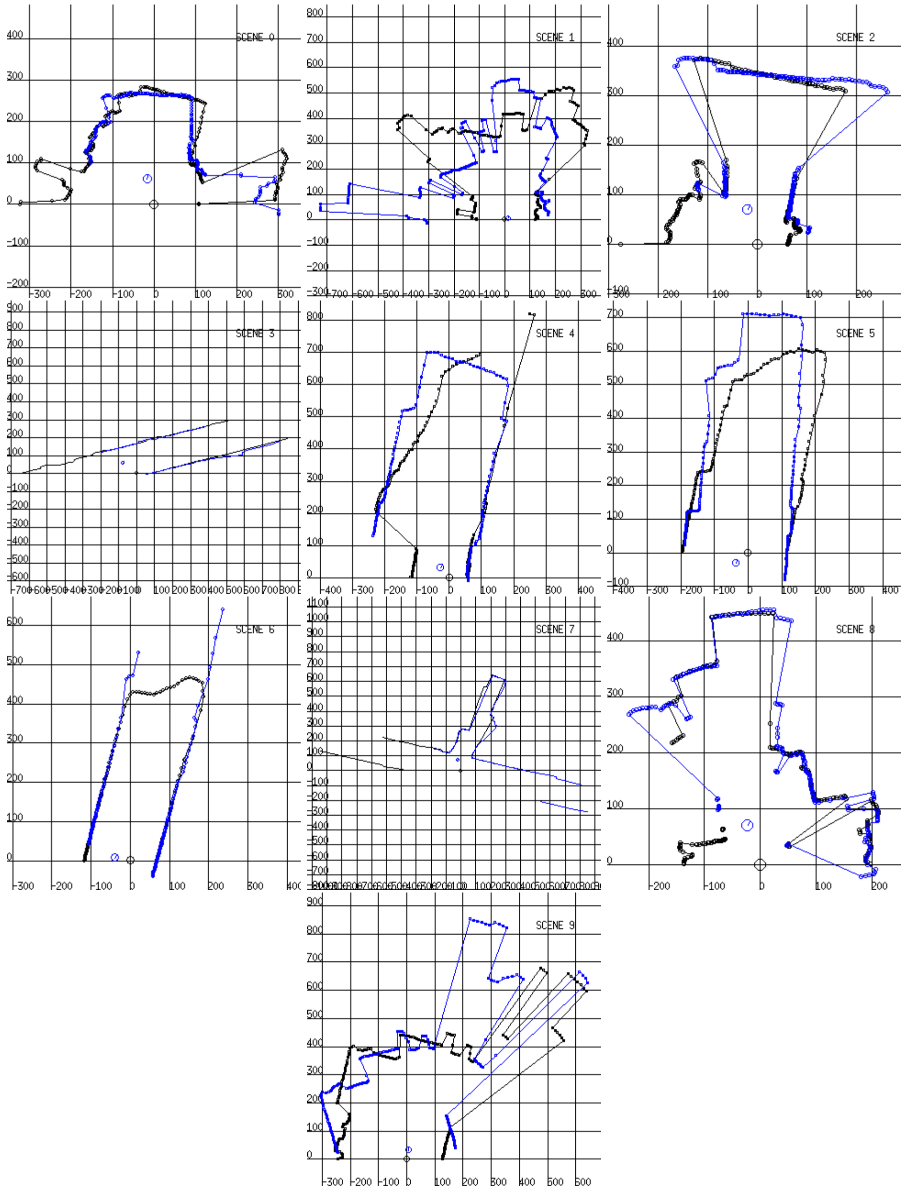

Figure 18: Scan match result for each scene for match number 3 in the experiment with ground truth using ICP.

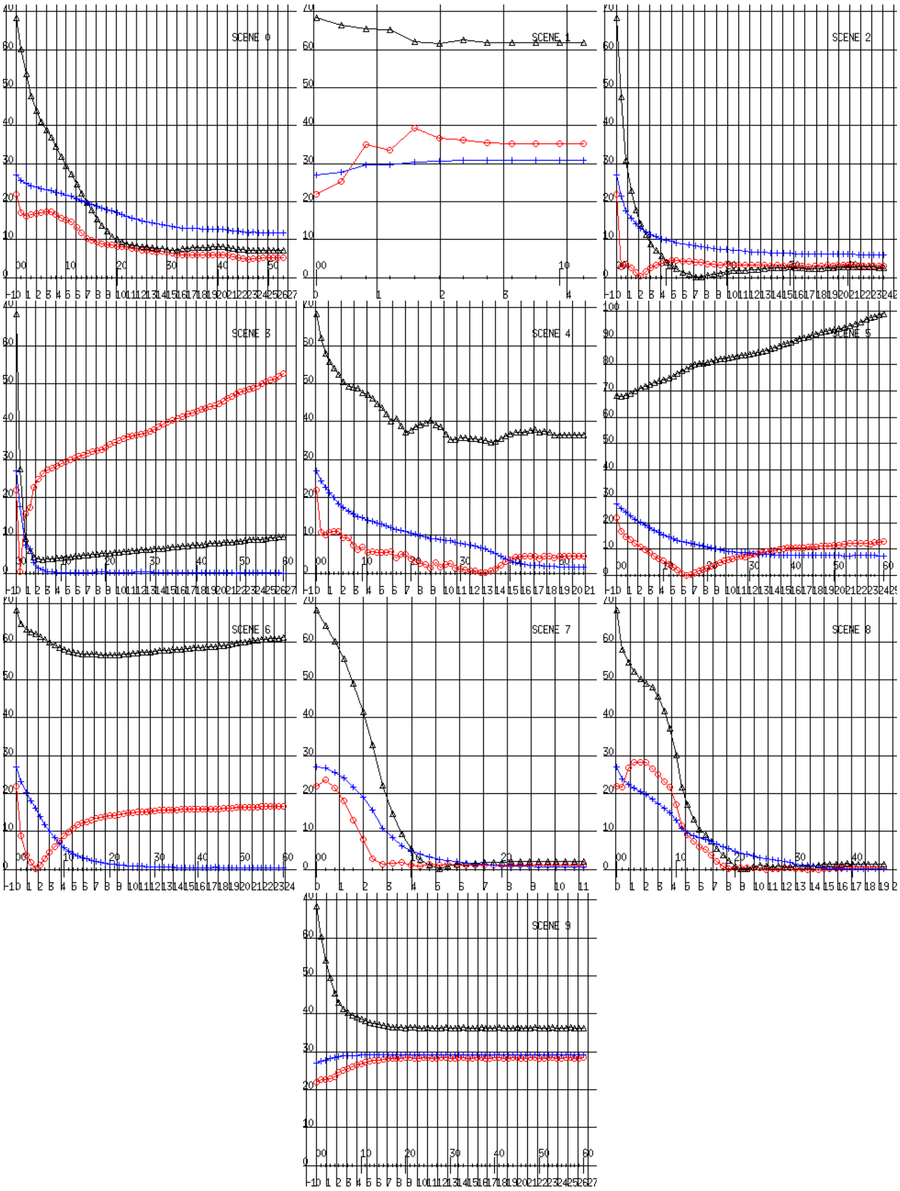

Figure 19: Match 3 scan match error evolution for each scene in the experiment with ground truth using ICP. Error in x (circles), y (triangles) and orientation (crosses) are expressed in $[cm]$ and $[°]$, respectively. Grid size is 1ms x 10cm and 1ms x 10°, respectively. Iterations are marked with small vertical lines on the horizontal axis. Each 10-th iteration is marked with a longer vertical line.

0	(0.9, 1.5, 0.3) 14, 2.7	(0.7, 0.4, 1.3) 16, 2.9	(1.1, 0.2, 0.1) 18, 3.3	(1.5, 0.4, 2.4) 20, 3.6	(0.6, 7.4, 0.2) 12, 2.2	(3.6, 0.1, 1.3) 12, 2.2
1	(5.1, 17.3, 5.5) 20, 3.7	(7.7, 13.1, 5.8) 28, 5.1	(0.4, 24.8, 8.3) 30, 5.5	(1.0, 1.5, 0.4) 27, 4.8	(0.3, 5.0, 0.6) 24, 4.3	(2.4, 0.5, 0.6) 12, 2.3
2	(0.4, 0.3, 0.3) 8, 1.5	(0.2, 0.6, 0.1) 24, 4.2	(0.5, 1.0, 0.3) 20, 3.6	(0.2, 0.9, 0.3) 20, 3.5	(0.2, 4.8, 0.3) 28, 4.9	(1.0, 2.7, 0.3) 12, 2.2
3	(9.7, 5.0, 0.2) 18, 3.2	(51.8, 25.3, 0.2) 12, 2.2	(22.1, 11.1, 0.3) 20, 3.6	(90.8, 19.4, 0.0) 30, 5.2	(24.3, 11.2, 0.1) 16, 2.9	(55.3, 46.3, 0.1) 30, 5.2
4	ERROR	(4.2, 47.9, 1.3) 20, 3.7	(0.9, 4.3, 0.0) 30, 5.1	(61.6, 160.3, 4.7) 30, 5.2	(73.8, 210.5, 1.5) 30, 4.9	(1.0, 6.1, 0.1) 30, 5.1
5	(0.6, 20.3, 0.4) 24, 4.4	(0.2, 24.0, 0.4) 30, 5.5	(1.3, 10.7, 0.4) 30, 5.4	(12.6, 49.3, 0.5) 30, 5.4	(3.6, 6.6, 0.9) 21, 3.8	(1.6, 4.6, 1.5) 19, 3.4
6	(1.4, 30.7, 0.3) 18, 3.3	(2.0, 63.0, 0.1) 16, 2.9	(2.7, 79.1, 0.2) 16, 3.0	(23.0, 85.2, 0.4) 30, 5.2	(21.8, 86.6, 0.3) 16, 3.0	(0.8, 4.7, 0.0) 9, 1.7
7	(0.2, 0.1, 0.0) 26, 4.7	(1.5, 0.2, 0.2) 16, 2.9	(0.1, 0.3, 0.1) 20, 3.6	(0.8, 2.6, 0.3) 18, 3.2	(0.9, 4.9, 0.1) 16, 2.9	(0.0, 0.6, 0.3) 15, 2.7
8	(0.7, 0.0, 0.0) 11, 2.0	(1.3, 2.1, 0.1) 22, 3.9	(0.1, 0.4, 0.3) 19, 3.3	(0.6, 0.6, 1.9) 22, 3.9	(0.0, 5.6, 0.9) 23, 4.0	(0.6, 0.4, 0.1) 12, 2.2
9	(3.7, 1.7, 0.8) 10, 1.9	(2.0, 0.4, 0.4) 18, 3.3	(1.4, 0.9, 0.2) 18, 3.3	(2.8, 3.0, 0.5) 18, 3.3	(1.6, 9.5, 0.7) 12, 2.2	(1.1, 1.6, 0.2) 13, 2.4

Table 5: Absolute errors in x[cm], y[cm], $\theta[^\circ]$, number of iterations and runtime [ms] of the PSM algorithm in the experiments with ground truth. Rows correspond to scenes 0–9, and columns correspond to matches 0–5.

0	(0.7, 1.6, 0.2) 13, 2.3	(0.8, 0.4, 1.4) 20, 3.5	(1.0, 0.1, 0.3) 13, 2.3	(1.6, 0.1, 2.4) 21, 3.6	(0.8, 6.7, 0.3) 13, 2.3	(3.4, 0.2, 1.2) 12, 2.1
1	(7.7, 19.2, 5.8) 10, 1.7	(7.0, 15.7, 6.3) 30, 4.9	(0.9, 25.8, 9.0) 30, 5.0	(1.4, 0.9, 0.4) 30, 4.9	(0.5, 5.2, 0.6) 25, 4.1	(1.0, 0.0, 0.4) 13, 2.1
2	(0.4, 0.2, 0.3) 9, 1.6	(0.3, 0.5, 0.3) 17, 2.8	(1.0, 0.4, 0.5) 12, 2.1	(0.2, 1.0, 0.4) 17, 2.9	(0.7, 5.1, 0.5) 10, 1.6	(1.0, 2.4, 0.3) 12, 2.1
3	(14.4, 7.5, 0.3) 8, 1.4	(49.2, 23.9, 0.3) 6, 1.0	(34.0, 17.1, 0.2) 6, 1.0	(55.1, 10.7, 0.2) 9, 1.5	(24.2, 11.1, 0.0) 6, 1.0	(28.5, 24.3, 0.2) 8, 1.6
4	(2.7, 46.7, 2.6) 17, 2.8	(6.1, 57.9, 1.6) 18, 3.0	(0.5, 10.7, 0.2) 18, 2.9	(51.7, 128.0, 5.3) 30, 4.8	(70.7, 117.7, 9.6) 30, 4.5	(6.2, 24.6, 0.2) 16, 2.6
5	(1.2, 16.7, 0.6) 17, 2.9	(0.1, 41.0, 0.4) 17, 2.9	(1.0, 24.3, 0.3) 21, 3.7	(13.7, 54.1, 0.4) 13, 2.2	(3.2, 2.5, 1.2) 24, 4.1	(0.9, 0.2, 0.7) 17, 2.9
6	(1.3, 23.2, 0.4) 17, 2.9	(1.6, 59.3, 0.3) 17, 2.8	(2.7, 73.0, 0.0) 13, 2.2	(19.0, 69.1, 0.3) 16, 2.6	(20.3, 79.8, 0.1) 17, 2.9	(1.1, 3.2, 0.3) 9, 1.8
7	(1.0, 0.1, 0.2) 14, 2.3	(1.0, 0.2, 0.2) 17, 2.8	(0.6, 0.1, 0.2) 13, 2.2	(1.5, 2.5, 0.3) 17, 2.8	(1.2, 4.9, 0.1) 13, 2.2	(0.1, 1.1, 0.2) 13, 2.2
8	(0.5, 0.6, 0.2) 13, 2.2	(1.1, 2.0, 0.4) 21, 3.5	(0.3, 0.4, 0.5) 18, 2.9	(0.6, 0.6, 1.9) 21, 4.1	(0.1, 5.7, 1.1) 24, 4.0	(0.2, 0.0, 0.1) 14, 2.3
9	(1.5, 1.6, 0.6) 13, 2.2	(1.5, 1.2, 0.2) 24, 4.1	(1.6, 2.3, 0.0) 13, 2.2	(2.4, 2.6, 0.1) 28, 4.7	(0.1, 5.2, 0.5) 20, 3.5	(0.8, 1.3, 0.2) 17, 2.9

Table 6: Absolute errors in x[cm], y[cm], $\theta[^\circ]$, number of iterations and runtime [ms] of the PSM-C algorithm in the experiments with ground truth. Rows correspond to scenes 0–9, and columns correspond to matches 0–5.

0	(1.5, 0.7, 0.9) 50, 23.8	(0.7, 1.2, 3.8) 60, 32.7	(1.1, 0.0, 0.5) 22, 11.4	(5.1, 7.2, 11.7) 53, 26.6	(0.4, 5.0, 1.4) 59, 29.8	(1.5, 0.6, 0.7) 56, 26.6
1	(7.6, 17.6, 6.1) 60, 26.8	(2.1, 0.4, 0.3) 33, 13.7	(12.5, 28.9, 9.4) 16, 6.8	(35.3, 61.9, 30.8) 11, 4.3	(2.0, 6.9, 0.3) 60, 25.8	(43.1, 68.4, 20.4) 34, 11.9
2	(0.5, 0.6, 0.4) 35, 17.5	(3.7, 10.1, 4.7) 32, 14.2	(0.1, 1.2, 0.5) 60, 28.7	(3.0, 2.7, 6.1) 47, 24.1	(1.0, 7.0, 0.5) 60, 27.9	(0.7, 1.6, 2.1) 60, 26.2
3	(3.6, 1.6, 0.2) 8, 3.5	(44.5, 22.0, 0.1) 22, 11.5	(51.3, 25.9, 0.6) 60, 29.3	(52.6, 9.6, 0.0) 60, 26.7	(49.4, 17.8, 0.0) 60, 28.4	(3.7, 3.6, 0.0) 60, 25.4
4	(1.9, 0.4, 2.3) 42, 18.0	(6.7, 63.2, 2.0) 22, 8.4	(6.2, 58.2, 1.4) 60, 22.9	(4.5, 36.3, 1.6) 55, 20.9	(8.0, 67.8, 2.6) 14, 5.5	(5.5, 23.0, 0.0) 28, 11.1
5	(0.2, 0.3, 0.2) 32, 13.6	(7.9, 84.8, 7.0) 60, 24.5	(0.3, 58.8, 0.2) 24, 10.9	(12.9, 99.1, 7.4) 60, 24.4	(14.0, 63.7, 0.1) 19, 10.0	(2.4, 9.6, 0.3) 45, 18.1
6	(0.0, 6.7, 0.0) 36, 17.4	(1.6, 63.7, 0.5) 31, 13.0	(2.0, 66.2, 0.3) 22, 9.6	(16.6, 61.0, 0.5) 60, 23.8	(16.8, 68.5, 0.4) 9, 4.4	(0.4, 2.8, 0.0) 26, 10.6
7	(0.1, 0.0, 0.1) 15, 6.4	(0.8, 0.8, 0.3) 28, 11.9	(0.5, 0.2, 0.1) 23, 9.9	(1.2, 2.2, 0.6) 29, 11.2	(0.4, 6.1, 1.9) 24, 12.5	(0.1, 0.3, 0.6) 31, 13.0
8	(0.5, 0.2, 0.4) 48, 20.4	(0.1, 0.6, 1.2) 25, 11.2	(1.3, 0.0, 1.0) 43, 19.4	(0.7, 1.3, 0.1) 45, 19.3	(2.0, 7.6, 2.0) 49, 22.9	(0.1, 0.6, 0.1) 60, 27.9
9	(0.7, 0.9, 0.5) 49, 22.6	(21.1, 52.7, 12.3) 60, 29.3	(0.5, 0.3, 0.4) 29, 13.0	(28.3, 36.2, 29.1) 60, 26.5	(1.4, 5.0, 1.0) 32, 15.3	(0.3, 0.7, 0.4) 60, 24.4

Table 7: Absolute errors in x[cm], y[cm], $\theta[^\circ]$, number of iterations and runtime [ms] of the ICP algorithm in the experiments with ground truth. Rows correspond to scenes 0–9, and columns correspond to matches 0–5.

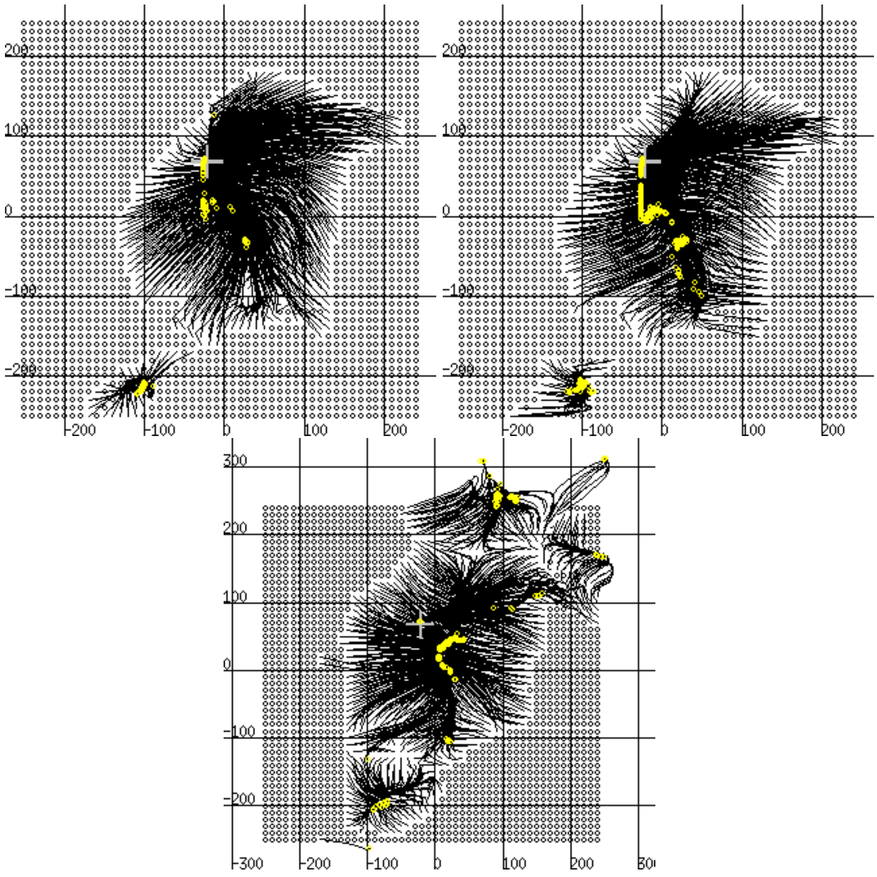

Figure 20: PSM, PSM-C and ICP convergence maps.

scene	PSM $[m^2]$	PSM-C $[m^2]$	ICP $[m^2]$
0	0.00	0.01	**0.79**
1	**3.52**	3.26	0.23
2	**2.34**	2.26	1.45
3	0.26	0.31	**0.49**
4	0.00	0.00	**0.12**
5	**0.96**	0.61	0.18
6	0.14	**0.26**	0.03
7	**4.01**	3.56	1.09
8	1.39	0.49	**4.36**
9	**7.11**	5.38	2.32
average	**1.97**	1.61	1.11

Table 8: Convergence areas for match 3 of all scenes for PSM, PSM-C and ICP.

enough to the true solution. Areas of convergence can be visualized by drawing the trajectory of the current scan into an image. To make visualization simpler just like in [Dudek and Jenkin, 2000] only the initial pose was changed.

Scan pairs from scenes 0-9, match 3 were selected for the convergence map experiment. Match 3 was selected in this experiment because of its large difference in the point of view (71cm, $27°$) for the current and reference scan. The initial position varied from -250cm to 250cm for x and y in 10cm increments. The initial orientation error was always 27°. The reason why the position is varied instead of the orientation is that (i) PSM can find the correct orientation quickly if the position is correct, therefore varying the orientation is not interesting, (ii) the large but constant initial orientation error chosen poses a challenge. The resulting convergence plots for scene 9 can be seen in fig. 20. Dark circles represent initial positions where the scan matching algorithms failed for the lack of associated points. Light colored circles represent final positions. Black lines correspond to the trajectories of the scans. Gray crosses mark the correct current scan positions.

When examining fig. 20, one has to keep in mind that in all scan matching implementations, associations having a larger error than one meter were discarded. To get an objective value for the performance of the implementations, the total number of matches and the number of successful matches were counted. Successful matches were matches with less than 10cm error in position and 2° in orientation[2]. The total number of scan matching trials was 2500 which corresponds to an area of $25m^2$. PSM had 711 successful matches which means that it converged to the correct solution from around a $7.1m^2$ area. PSM-C had 538, giving $5.38m^2$. ICP had 232 correct ones which corresponds to $2.32m^2$.

A non-graphical representation of all the results can be seen in tab. 8. From this table one can observe that PSM has the largest average area of convergence followed by ICP and PSM-C. The area of convergence of PSM was in 5 cases larger than that of ICP. The small areas of convergence from scenes 3-6 were due to the corridor like character of the scenes, where the lack of features limit the accuracy of scan matching results in the along corridor direction. The 0 area of convergence in scene 0 was caused by a minimum for orientation with $2.4°$ error just at the vicinity of the correct pose.

From this experiment one can conclude, that on average the implemented PSM converged from a larger area than ICP when using the dataset for scene 0-9, match 3. PSM-C performed slightly worse than PSM, but better than ICP.

3.5 SLAM

A simple implementation of Kalman filter SLAM was programmed in C++ to evaluate the practical usability of the described scan matching method. The description in [Davison, 1998] was followed at the implementation of the Kalman filter SLAM. As in [Bosse *et al.*, 2004] laser scanner poses were used as landmarks. With each landmark the associated laser scan was also stored. Each time the robot got to a position which was further than one meter from the closest landmark, a new landmark was created. Each time the robot got closer than 50cm and $15°$ to a landmark not updated in the previous step, an update of the landmark was attempted. Consecutive scans were not matched. This is because the short term odometry of our robot when traveling on flat floors is more accurate (see section 3.6) than the implemented scan matching algo-

[2] In the case of unsuccessful matches, the scan matching process either converged to local minima or diverged. In a simplified view one can imagine that the points of a fixed reference scan are connected to the associated points of the current scan with rubber strings. Convergence to a local minimum occurs, when for given associations the net force on the current scan equals zero.

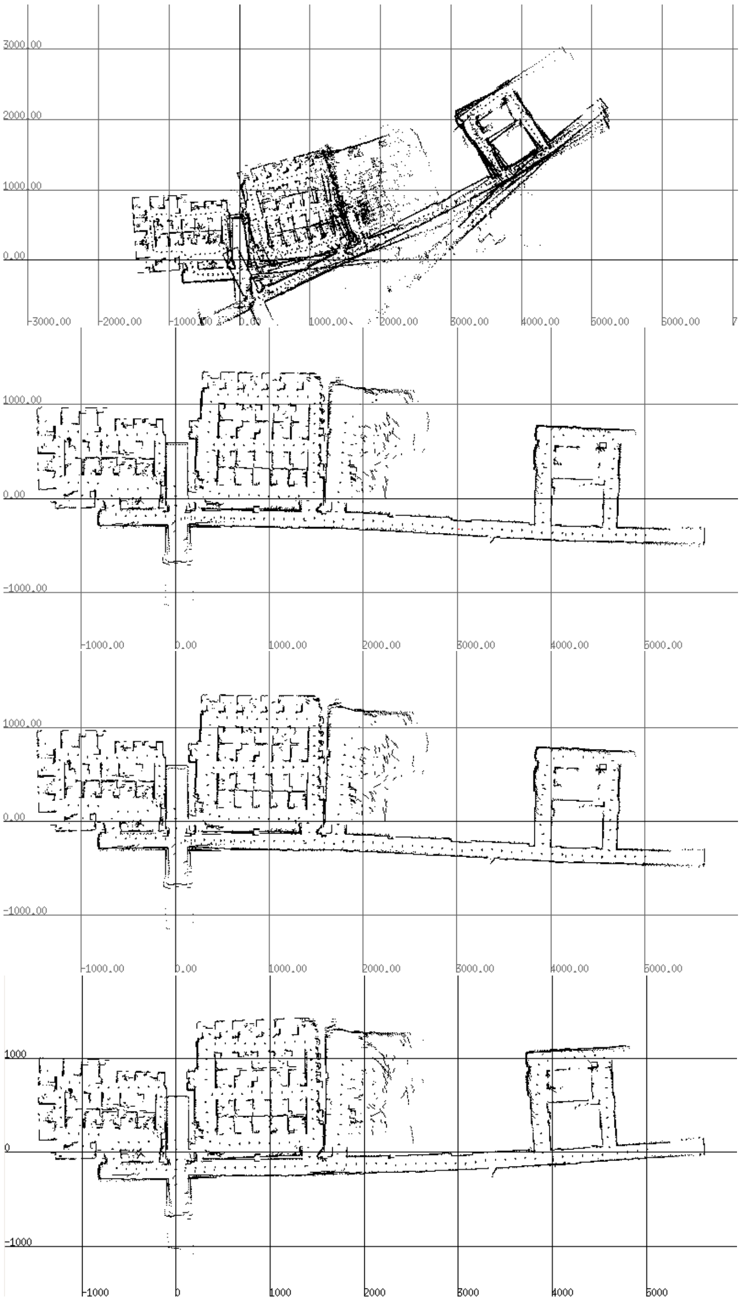

Figure 21: Maps resulting from odometry only, SLAM with PSM, PSM-C and ICP. Grid size is 10x10m.

rithms applied to data from the robot's laser range finder. Because Kalman filter SLAM requires an error estimate for the scan matching result, a simple error model was implemented, where a preset covariance matrix is scaled with the square of average absolute range residual. For non-corridor areas a diagonal preset covariance matrix was used. For corridor like areas, a non-diagonal matrix was chosen to express the larger along-corridor uncertainty. The classification of scans to corridor and non-corridor like areas was done by using the variance of orientations of line segments obtained by connecting neighboring points of a scan. More on our SLAM implementation can be read in [Diosi and Kleeman, 2005].

The raw data set used in the Kalman filter SLAM is shown in fig. 21. The structures in the middle of the two rooms on the left are office cubicles. The third room is a seminar room filled with tables and chairs. The table and chair legs appear as a randomly distributed point cloud. The robot was equipped with one SICK LMS 200 and odometry and started from the corridor intersection between the 2 rooms on the left. It visited the left room, and after one loop, it proceeded through the corridor to the middle room where it performed a large and a small loop and continued to the third (seminar) room. In the third room the robot was twice driven over a 1.5cm high cable protector on the floor at 40cm/s and at 20cm/s speed. After the visit to the third room the robot returned to its initial location from which it traveled to the far end of the corridor, went around a loop and came back. During the traversal of the environment, no less than 10 people walked in the view of the laser scanner and some doors were opened and closed. Considering the presence of walking people, repetitive cubicles, long corridors and 2 collisions with an obstacle on the floor, this dataset is not the most ideal for mapping.

The SLAM results are shown in fig. 21. The SLAM results are significantly better than those from odometry only (fig. 21, top). All three scan matching approaches performed similarly. The odometry of the robot was reasonably calibrated. This was necessary to be able to perform loop closing in the repetitive cubicle environment of the second room without the implementation of special loop closing algorithms.

In the C++ implementation of scan matching and SLAM, the 20 minutes worth of data consisting of 46×10^3 scans and 12×10^4 odometry readings took about 2 minutes

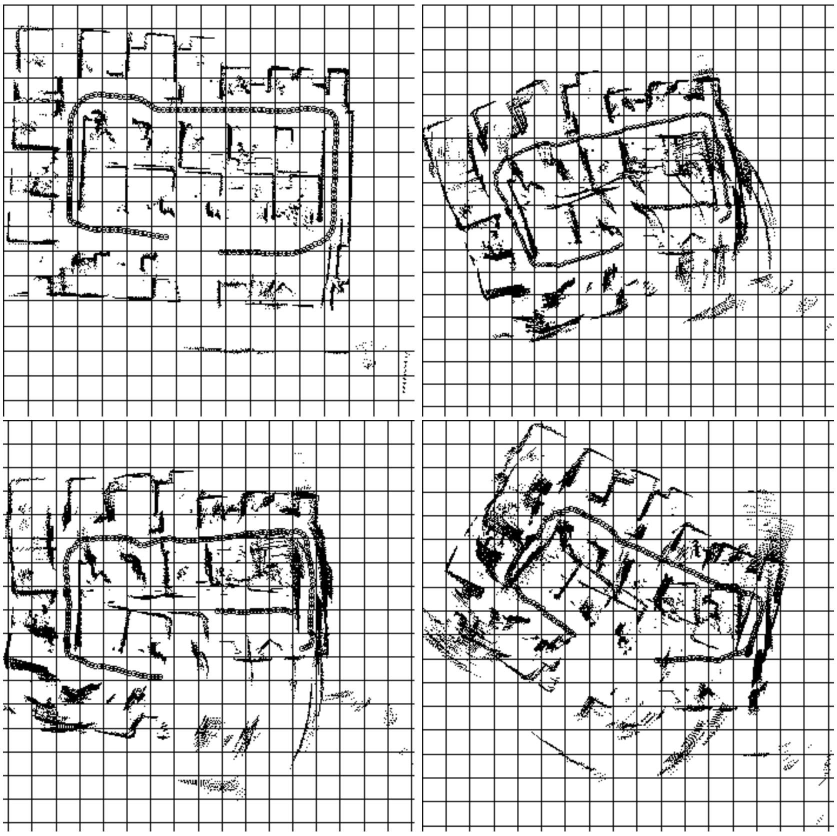

Figure 22: The alignment of scans using odometry (top-left), PSM (top-right), PSM-C (bottom-left) and ICP (bottom-right). Grid size is 1x1m.

to process on a 900MHz Celeron laptop for all variants. There were 100 successful (no divergence) scan matches for PSM SLAM variant with an average of 3.1ms scan matching time. There were 100 scan matches with PSM-C, with 2.1ms average time. ICP was successfully used 67 times with an average of 20.2ms.

3.6 Scan Matching vs Odometry

To support the statement in the previous section about the accuracy of our robot's odometry with respect to scan matching, a simple comparison of odometry and the implemented scan matching algorithms was performed.

In this experiment, data logged in the leftmost room in the SLAM experiment (fig. 21) was used. Laser scans aligned using the pose derived from odometry are shown in fig. 22. In the same figure the laser scans aligned with matching consecutive laser scans (logged at more than 30Hz) using PSM, PSM-C and ICP are also shown. Unlike in previous experiments, the scan matching approaches were run for 1000 iterations, which is much longer than required for convergence, in order to show the behavior when the number of iterations is unlimited. Figure 22 displays scans and robot poses every 0.5 seconds.

By observing fig. 22 it is clear that the results obtained by odometry outperform scan matching in this experiment. None of the scan matching approaches produced a good result. One of the problems in the scan matching results is that the right side of the room is misrepresented. The error was due to the robot travelling from the bottom right corner to the top right corner through a narrow corridor between a partition and the wall. At some places in this narrow corridor all but 8 points from 181 points were on the side walls. These 8 points were not enough to correctly align the along corridor position of the robot. The ICP implementation was more disadvantaged than the other approaches because in the implementation, only the best 80% of the point correspondences were used in the pose calculation. PSM and PSM-C suffered from drift after the robot performed the turn at the bottom right corner. After the turn all but a few points were on the right-side wall which contained only one corner. In this case the 1000 iterations were enough to cause a significant drift over several scan matches. The drift appears as a discontinuity in the robot's position (shown by circles) in the bottom right corner. Better results with all three scan matching approaches were obtained when every 10th scan was matched, because with a smaller number of scan matches less drift accumulates. PSM and PSM-C results were better if matching was stopped when the pose change of the current scan became small, because in this case the drift in the corner did not appear at all. When PSM was run with the parameters used in the rest of the experiment the resulting map was better than that in fig. 22. Even after extensive trials, no set of parameters could be found that outperformed the results using robot odometry.

3.7 Discussion

The goal of the experiments was to give an objective evaluation of PSM, PSM-C and ICP in a variety of real environments. To ensure objectiveness during the tests, all parameters values of PSM and PSM-C were the same. Parameters shared between PSM and ICP were also the same including the search window size, except the termination condition.

One can compare scan matching algorithms in different ways: one can run them for a given time and observe which one has the smallest pose error, or one can run them for a given number of iterations. We have chosen a third possibility where we have set the parameters for the terminating condition to achieve approximately the same accuracy in a simulated experiment. Having approximately the same accuracy enabled us to investigate convergence time, number of iterations and the area of convergence. Because ICP converges slower than PSM and PSM-C the terminating conditions of ICP i.e. the threshold on pose change and the maximum number of iterations were changed. The rest of the shared parameters had identical values. PSM had only one parameter, PM_C which ICP did not. The only parameter which ICP had and PSM did not was the percentage of the worst point matches to be discarded.

The simulation results indicate that PSM and PSM-C can converge in much shorter time and in much less iterations than ICP while obtaining the same accuracy. These indications were then confirmed in the experiment with ground truth in which 60 matches were performed in different environments. PSM was on average nearly 6 times (PSM-C more than 7 times) faster than ICP (see tab. 4). The number of iterations for PSM were 2.3 times (PSM-C 2.7 times) less than for ICP. This ratio would have been even better if one orientation and one translation step would have been counted as 1 iteration as in IDC instead of 2. Table 4 indicates that ICP is much more inaccurate than PSM. However a close examination of lines 0–2 and 7–9 of tab. 7, reveals that ICP converged to incorrect solutions far from the correct ones more often than PSM. If these cases are ignored, then the accuracy of PSM and ICP was very similar in the experiments. Having a similar accuracy is important because our comparison is based on an equal accuracy requirement. The large number of convergences of ICP to a far away solution indicate that ICP has a smaller area of convergence than PSM. The convergence map experiment confirms this hypothesis. In the area of convergence experiments on average PSM converged from almost double the area (PSM-C 1.45 times) than that of ICP.

The reason why PSM needs less time for each iteration than ICP is because the correspondences are chosen using a matching bearing criterion, thus no search for corresponding points is necessary for translation calculation. The orientation calculation step which is of O(kn) complexity is inexpensive as well. However ICP needs to search for corresponding points what has a complexity of O(kn) if the search window is limited. The search in ICP involves much more operations than that in the orientation estimation step of PSM, therefore in our case with 181 scan points, each iteration of PSM was much faster than that of ICP.

PSM did not only need less time for each iteration but it also needed less iterations. The pose estimation step in PSM can estimate the position of the current scan in a few steps if the correct orientation is known. The orientation estimation step on the other hand can estimate the correct orientation in one step if a correct pose is given. The orientation estimation step had one more great advantage beside its quickness. It searched through a $\pm 20^\circ$ interval for the most suitable orientation, which enabled it to move the pose out of local minima. One can see the effect of the orientation search on the PSM-C algorithm in fig. 17 where in most graphs there is large orientation reduction in the 4-th iteration where the orientation search is first performed.

In the experiments the search window for the PSM orientation estimation was chosen to be $\pm 20^\circ$. Choosing a small window may slow down the convergence and limit the ability to jump out from a local minimum. Choosing a large window may unnecessarily increase the processing time. Large search windows may allow convergence to wrong solutions as well. A $\pm 90^\circ$ search window may allow convergence to an orientation off by 90°, due to the rectangular nature of rooms.

One would intuitively think, that in cases with a large initial orientation error one would benefit from enlarging the orientation search window beyond the initial angular error. However, this may not always be the case. Match 3 in the ground truth experiments contained an initial error of $27°$. Surprisingly the extension of the search window from $20°$ to $30°$, did not result in significant reduction in the number of iterations. We have investigated scenes 0-3. Even though, in most of the cases the orientation error was reduced to $1° - 2°$ in the first orientation estimation step, the position estimation could not follow.

Interpolation in the orientation search helps to increase the orientation estimation accuracy beyond the angular resolution of the laser range finder. Surprisingly the presence of interpolation does not make a significant difference in the performance of PSM on the ground truth dataset when the orientation search is performed at $\Delta i = 1°$ increments. At $\Delta i = 4°$, however without interpolation PSM's average orientation error rose to $1.64°$ (originally $0.84°$). The average displacement error became 4.6cm (originally 3.8cm). The use of interpolation reduced the orientation error to $1.2°$ and the displacement error to 3.9cm. This indicates, that with the use of interpolation one can further reduce the run time of PSM without substantially decreasing the accuracy. This can be achieved by increasing the interval in between consecutive error calculations. Alternative ways for changing Δi have not been investigated.

As mentioned in section 2.3 the pose estimate of PSM (and therefore PSM-C) may drift on featureless corridors. This can be seen in fig. 14 at scene 3. The drift is apparent from the constant rate position change while having an orientation error close to 0. The amount of drift at scene 3, match 3 was only 22cm. Drift is not only a problem for PSM but for ICP as well as it can be seen in fig. 18, where the position drifted 25cm. However we did not notice any drift when ICP was implemented without interpolation. The experienced drifts were small in most cases, and we do not consider them as an important factor since on featureless corridors we can not determine the correct along corridor position. In the SLAM experiment we have handled corridors by detecting them and by modeling the scan matching error with a very large error in the direction of the corridor.

Some scan matching approaches which employ different strategies for estimating orientation and position can converge to an oscillatory state, i.e. to a limit cycle. When the 3 implemented scan matching algorithms were run for 1000 iterations, we were able to find examples of limit cycles for all 3 of them. However, the limit cycles were at least an order of a magnitude smaller than the errors in the estimated poses, therefore we did not investigate any further.

It is clear that PSM grossly outperformed the implemented ICP, but how would it fare compared to other point to point scan matching approaches? MbICP [Minguez *et al.*, 2006] is a recent high performing approach. In fig. 4 of [Minguez *et al.*, 2006], MbICP's runtime and number of iterations are compared with ICP's. The figure can be interpreted to mean that MbICP needs only 66% of ICP's number of iterations to converge. The runtime of MbICP appears to be 75% of ICP's. In our ground truth experiment, the difference between ICP and PSM was much larger (see tab. 4). PSM needed only 44% (PSM-C 37%) of ICP's number of iterations to converge. The difference in runtime was even more dramatic. PSM needed only 17% of ICP's runtime, and PSM-C needed 13%.

The performance of PSM and PSM-C were similar albeit PSM-C was faster in the tests and PSM had a larger area of convergence. Both PSM and PSM-C use the matching bearing association rule to select corresponding points. Both approaches minimize the sum of square range residuals. The difference between PSM and PSM-C lies in the way this minimization is performed. In PSM the position is estimated by applying linear regression to the linearized transformation which transforms current scan points into the reference scan's polar coordinate frame. Orientation is sought by shifting the current scan left and right until best match with the reference scan is found. In PSM-C pose estimation is performed using similar equations as in ICP. Every fourth iteration is the same orientation estimation step as in PSM. The choice between PSM and PSM-C should depend on the requirements for the system. If one needs high speed then one should choose PSM-C. For applications requiring larger area of convergence, the PSM is the right choice.

The purpose of the SLAM experiment was to test PSM in an application. Even though the detection and tracking of moving objects was not implemented, the system tolerated moving persons during the experiment. Moving persons can have a bad effect on the scan matching result if they are represented by many points, and if they are close to an another object. In this case points representing the human can be associated to the points representing the other object. The same considerations apply to table and chair legs which were not removed by the median filter.

In the SLAM experiment several small loops were successfully closed. Had the loops been large, the local laser scan matching approaches would not have been able to close the loops. However due to their high speed, PSM and PSM-C may be used to close larger loops. Whenever the current scan can be associated to several reference scans from the map, the current scan should be matched with all of them with the initial poses set to 0. One should only update the state of the Kalman filter when a unique match is found. Such an approach for loop closure may work because PSM enables hundreds of scan matches per second even on slow computers. The second reason why this approach may work is because in most buildings it is reasonable to expect that robots will pass approximately the same path twice when closing a loop. This means, that there will be current scans which were taken in the proximity of some of the reference scans stored in the map. If a reference scan was taken within the convergence area of the current scan, then the two scans can be matched by setting the initial poses of the current and reference scan to 0, thus ignoring the robot pose estimate which may contain a large error.

4 Conclusions and Future Work

In this paper a laser scan matching method is proposed which works with the laser measurements in their native, polar form. The polar scan matching (PSM) approach belongs to the class of point to point matching algorithms. PSM takes advantage of the structure of laser scanner measurements by operating in the laser scanner's polar coordinate system. The direct use of range and bearing measurements coupled with a matching bearing association rule and a weighted range residual minimization, results in an $O(n)$ complexity pose estimation approach and an $O(kn)$ complexity orientation estimation approach. In $O(kn)$ of the orientation estimation approach, k is proportional to the angular resolution of the laser scans. Opposed to the $O(n^2)$ projection filter of [Gutmann, 2000], preprocessing of scans is done with $O(n)$ complexity if there are no occlusions in the current scan when viewed from the reference scan's position. A variant of PSM, PSM-C is also introduced where the translation estimation step of PSM is replaced with a weighted variant of the pose estimation equations from [Lu and Milios, 1997]. In PSM-C due to the use of the matching bearing rule, equations from [Lu and Milios, 1997] also minimize the sum of square range residuals. For comparison, an ICP scan matching algorithm has been implemented.

Simulation of matching scans in a room demonstrates that the current scan pose error decreases more quickly with PSM and PSM-C to a small value, than with our ICP implementation. Scan matching experiments using real scans were performed with a SICK LMS 200 in a variety of environments. Comparison of the results with ground truth revealed that in the tests, the performance of PSM and PSM-C surpasses that of our ICP implementation in speed. However when matching corridors, a position drift in the direction of the corridor has been observed with PSM. This drift was also observed when using PSM-C or ICP. A comparison of areas of convergence for PSM, PSM-C and ICP were performed. It was found, that PSM converged to the correct solution from a larger area than PSM-C and our ICP implementation.

The usability of the proposed scan matching approaches has been tested by performing Kalman filter SLAM with scan matching in a static environment. The maps created by PSM and PSM-C are ICP are similar in quality as shown in fig. 21. In fig. 21, the quality of the maps can be judged by the straightness of the corridor and by the presence of walls with multiple representations.

As future work, the tracking and tagging of moving objects could be considered. The real advantage of the efficient PSM over other methods which employ search to find corresponding points becomes more apparent when the number of points is large. One such case is in 3D scan matching. It would be interesting to know if PSM could be adapted to 3D. The projection filter and position estimation would be still of $O(mn)$ and $O(n)$ complexities, respectively. Estimation of the 3 orientation angles if done sequentially would still result in $O(kn)$ complexity, where k is proportional to the number of range readings per unit angle. Even though 3D scan matching with a modified PSM is an exciting problem, due to the lack of time we have to consider it as possible future work.

Acknowledgment

We acknowledge the financial support of the ARC Centre for Perceptive and Intelligent Machines in Complex Environments. Steve Armstrong is gratefully acknowledged for technical support. Alan Zhang's feedback regarding the PSM source code is appreciated. The reviewers are gratefully acknowledged for improving this paper with their comments.

References

[Besl and McKay, 1992] P. J. Besl and N. D. McKay. A method for registration of 3D shapes. *IEEE Transactions on Pattern Analysis and Machine Intelligence*, 14(2):239–256, 1992.

[Biber and Straßer, 2003] P. Biber and W. Straßer. The normal distributions transform: A new approach to laser scan matching. In *IROS'03*, volume 3, pages 2743–2748. IEEE, 2003.

[Bosse *et al.*, 2004] Michael Bosse, Paul Newman, John Leonard, and Seth Teller. Simultaneous localization and map building in large-scale cyclic environments using the Atlas framework. *The International Journal of Robotics Research*, 23(12):1113–1139, 2004.

[Censi *et al.*, 2005] A. Censi, L. Iocchi, and G. Grisetti. Scan matching in the Hough domain. In *Proceedings of the 2005 IEEE Int. Conf. on Robotics and Automation*. IEEE, 2005.

[Censi, 2006] A. Censi. Scan matching in a probabilistic framework. In *Proceedings of the 2006 IEEE Int. Conf. on Robotics and Automation*. IEEE, 2006.

[Cox, 1991] I. J. Cox. Blanche–an experiment in guidance and navigation of an autonomous robot vehicle. *IEEE Transactions on Robotics and Automation*, 7(2):193–203, april 1991.

[Davison, 1998] A. Davison. *Mobile Robot Navigation Using Active Vision*. PhD thesis, University of Oxford, 1998.

[Diosi and Kleeman, 2005] A. Diosi and L. Kleeman. Scan matching in polar coordinates with application to SLAM. Technical Report MECSE-29-2005, Department of Electrical and Computer Systems Eng., Monash University, 2005. Available: http://www.ds.eng.monash.edu.au/techrep/reports/.

[Dudek and Jenkin, 2000] G. Dudek and M. Jenkin. *Computational Principles of Mobile Robotics*. Cambridge University Press, Cambridge, 2000.

[Gutmann, 2000] J.-S. Gutmann. *Robuste Navigation autonomer mobiler Systeme*. PhD thesis, Albert-Ludwigs-Universität Freiburg, 2000.

[Hähnel *et al.*, 2003] D. Hähnel, W. Burgard, D. Fox, and S. Thrun. An efficient fast-SLAM algorithm for generating maps of large-scale cyclic environments from raw laser range measurements. In *IROS'03*, volume 1, pages 206–211. IEEE, 2003.

[Jensen and Siegwart, 2004] B. Jensen and R. Siegwart. Scan alignment with probabilistic distance metric. In *Proc. of 2004 IEEE/RSJ Int. Conf. on Intelligent Robots and Systems*. IEEE, 2004.

[Kay, 1993] Steven M. Kay. *Fundamentals of Statistical Signal Processing*, volume 2. Estimation Theory. Prentice Hall, New Jersey, 1993.

[Lingemann *et al.*, 2004] K. Lingemann, H. Surmann, A. Nüchter, and J. Hertzberg. Indor and outdoor localization for fast mobile robots. In *IROS'04*, volume 3, pages 2185–2190. IEEE, 2004.

[Lu and Milios, 1997] F. Lu and E. Milios. Robot pose estimation in unknown environments by matching 2D range scans. *J. of Intelligent and Robotic Systems*, 20:249–275, 1997.

[Lu, 1995] Feng Lu. *Shape Registration Using Optimization for Mobile Robot Navigation*. PhD thesis, University of Toronto, 1995.

[Menegatti *et al.*, 2006] E. Menegatti, A. Pretto, A. Scarpa, and E. Pagello. Omnidirectional vision scan matching for robot localization in dynamic environments. *IEEE Transactions on Robotics*, 22, no. 3:523–535, June 2006.

[Minguez *et al.*, 2006] J. Minguez, L. Montesano, and F. Lamiraux. Metric-based iterative closest point scan matching for sensor displacement estimation. *IEEE Transactions on Robotics*, 22, no. 5:1048–1054, October 2006.

[Montesano *et al.*, 2005a] L. Montesano, J. Minguez, and L. Montano. Modeling the static and the dynamic parts of the environment to improve sensor-based navigation. In *IEEE International Conference on Robotics and Automation (ICRA)*, pages 4556–4562, Barcelona, Spain, 2005.

[Montesano *et al.*, 2005b] L. Montesano, J. Minguez, and L. Montano. Probabilistic scan matching for motion estimation in unstructured environments. In *IROS'05*, pages 3499–3504, 2005.

[Nishino and Ikeuchi, 2002] K. Nishino and K. Ikeuchi. Robust simultaneous registration of multiple range images. In *The 5th Asian Conference on Computer Vision*, 2002.

[Thrun *et al.*, 2000] S. Thrun, W. Burgard, and D. Fox. A real-time algorithm for mobile robot mapping with applications to multi-robot and 3D mapping. In *ICRA'00*, volume 1, pages 321–328. IEEE, 2000.

[Tomono, 2004] M. Tomono. A scan matching method using Euclidean invariant signature for global localization and map building. In *ICRA'04*, volume 1, pages 886–871. IEEE, 2004.

[Weiss and Puttkamer, 1995] G. Weiss and E. Puttkamer. A map based on laserscans without geometric interpretation. In *Intelligent Autonomous Systems - 4*, pages 403–407, Germany, 1995.

[Ye and Borenstein, 2002] C. Ye and J. Borenstein. Characterization of a 2-D laser scanner for mobile robot obstacle negotiation. In *Proceedings of the 2002 IEEE International Conference on Robotics and Automation*, pages 2512–2518, Washington DC, May 2002. IEEE.